Features Extraction in Healthy and Diabetic Retinopathy Retinal Images

By

Akande Noah Oluwatobi
B. Tech., M. Tech. (Ogbomoso)
(16/68HG003)

SUPERVISOR: DR. (MRS.) OLUWAKEMI C. ABIKOYE

BEING A Ph. D. RESULT SEMINAR REPORT SUBMITTED TO THE DEPARTMENT OF COMPUTER SCIENCE, FACULTY OF COMMUNICATION AND INFORMATION SCIENCES, UNIVERSITY OF ILORIN, NIGERIA

OCTOBER, 2018.

TABLE OF CONTENTS

1. BACKGROUND TO THE STUDY

Security systems are needed to guarantee confidentiality, maintain integrity and ensure availability of individual's or organization's sensitive data, information and personal effects from unauthorized access, use, disruption, disclosure, modification, or destruction. Though several security systems exist, biometric security systems have been proven to be accurate and reliable to a high degree (George, Karthick & Harikumar, 2014). A biometric security system is a pattern recognition system that compares a registered biometric trait with a query biometric trait with a view to authenticate the claim of an individual to a possession (Sadikoglu & Uzelaltinbulat, 2016). They employ unique human physical, behavioral and chemical characteristics in identifying and authenticating the user of a biometric system. These unique biometric attributes provide better security since they cannot be lost, transferred or stolen; they are not needed to be remembered by the carrier, they are difficult to forge and also require the presence of the genuine user when granting access to a particular resource (Unar, Seng & Abbasi, 2014). Biometric systems are named with respect to the biometric traits to be used for authentication. Hence, they could be fingerprint, palmprint, face, iris, retina or gait recognition system.

With retinal biometric system in focus, features extracted from the retina is used to verify and authenticate the identity of an individual. These features could be extracted from various components of the retina such as blood vessels, optic disk, fovea and macula (Geetharamani & Balasubramanian, 2016). Individual's retina is unique as no two individual can have the same pattern of blood vessels on their retina; even identical twins have distinct patterns (Frucci, Riccio, Sanniti & Serino, 2016). It cannot be duplicated and do not change over time (Pouya & Pourghassem, 2017). Furthermore, when compared to other biometric systems, retina biometric system has the lowest error rate (Nixon, Aimale & Rowe, 2008). Among all the

biometric systems, only retina based biometric system remains unforged (Frucci et al., 2016) as the retina of a deceased person decays too rapidly to be used to deceive a retinal scan.

Despite all these advantages, the accuracy of retina recognition system is being greatly undermined by several diseases; the most prevalent being Diabetic Retinopathy (DR) (Waheed et al., 2016). DR is a common micro vascular complication of diabetes (Hendrick, Gibson & Kulshreshtha, 2015) which is capable of damaging the blood vessels and could further lead to total blindness of the eye. Moreover, the prevalence of DR is expected to grow exponentially and affect over 300 million people worldwide by 2025 (Adalarasan & Malathi, 2018) (Sidibé, Sadek & Mériaudeau, 2015) which may certainly have adverse effect on retina recognition systems. Since, the presence of these diseases do complicate recognition task to a great extent (Waheed et al., 2016), research efforts have been focused on developing retina biometric systems that will be resistive to the effects of DR.

2. STATEMENT OF THE PROBLEM

In this era of cutting-edge technology, demand for a reliable security system is increasing likewise biometric security systems which employs unique human physical and behavioral traits in identifying and authenticating the user of a biometric system. Among these traits, human retina is the most stable, reliable and secured biometric trait for human authentication and verification (Nigam, Vatsa, & Singh, 2015; Panchal, Bhojani, & Panchal, 2016; Pouya & Pourghassem, 2017). Its non-exposure to the environment and swiftness of decay in dead persons makes it difficult to forge. A retinal biometric system takes into account these properties as well as the invariant structure of patterns present on retinal blood vessels to establish individual's identity (De Marsico, Frucci & Riccio, 2016).

However, human retina is not resistive to certain diseases including Diabetic Retinopathy (DR), hypertension, Glaucoma, high blood pressure, autoimmune deficiency syndrome,

arteriosclerosis and cardiovascular disease (Nigam et al., 2015). DR being prevalent among these diseases has been shown to cause measurable changes in the retinal blood vessels' diameter (Abbadi & Saadi, 2014), branching angles, width, tortuosity and length (Sadikoglu & Uzelaltinbulat, 2016). This have been revealed to have adverse effect on the identification process and eventual accuracy of retinal biometric system (Waheed et al., 2015). Since, the reliability and efficiency of any biometric system is dependent on the accuracy of its features extraction stage (Panda, Puhan & Panda, 2016), research efforts aimed at improving the recognition rate or accuracy of retinal biometric system must first improve its features extraction accuracy.

In this regards, several techniques aimed at improving the accuracy of retina biometric systems have been reported in the literature. Most of these techniques have employed different algorithms or hybridized algorithms for better features extraction from diseased or healthy retinal images (Isabel et al., 2016; Panchal et al., 2016; Pouya & Pourghassem, 2017; Rodrigues & Marengoni, 2017). However, most works reported so far have yielded a recognition system that could either recognize diabetic or healthy retinal images and not both (Holbura, Gordan & Vlaicu, 2012; Lumini & Nanni, 2017; Waheed et al., 2016). As a result of this, if healthy retinal images of an individual was employed in developing the recognition system, any change in state of the health status of the individual will affect the recognition accuracy of the biometric system. Similarly, if retinal images from a DR individual was employed to develop the biometric recognition system, any change in the stages of DR will affect the recognition accuracy of the biometric system. Therefore, this research intends to extract features from both healthy and unhealthy retinal images as a preliminary stage towards coming up with a retinal recognition system that will be able to recognize the retinal of a healthy as well as DR individual.

3. AIM AND OBJECTIVES

The aim of this research is to come up with an enhanced recognition system for healthy and diabetic retinopathy retinal images. The specific objectives are to:

i. Extract structural features from healthy retinal images using statistical techniques.

ii. Locate and remove optic disk from diabetic retinopathy retinal images using morphological operations

iii. Extract morphological and lesion based features from diabetic retinopathy retinal images using connected component analysis and statistical techniques respectively.

iv. Employ Matlab programming tool to implement a retina recognition system using the extracted features.

v. Evaluate the performance of the retina recognition system using recognition rate, sensitivity and specificity.

4. LITERATURE REVIEW

4.1 Overview of Biometric Systems

Authenticating the identity of an individual is one of the expected objectives of security systems. This could be achieved with the use of traditional methods such as passwords, Personal Identification Numbers (PINs), tokens and smart identification cards. These methods are not efficient as passwords and PINs can be forgotten or divulged to an unauthorized person while smart cards and tokens can be lost or stolen; hence, they do not provide a reliable means of identity recognition. With a view to overcome these challenges, identification systems using human physical, behavioral and chemical attributes termed “biometrics” are being used to authenticate and verify the identity of an individual (Jain, Nandakumar & Ross, 2015).

For an attribute to be appropriate as a biometric trait, such must satisfy the following criteria as submitted by Unar et al., (2014): (i) universality which stipulates that an ideal biometric trait must be possessed by all humans, (ii) distinctiveness which specifies that a perfect biometric trait must be distinct from others of its kind. (iii) invariance which ensures that the carefully chosen biometric attribute must remain unchanged with time (iv) collectability which specifies that the samples of the preferred biometric trait must be easy to acquire in terms of acquisition and digitization (v) performance which dictates that the favourite biometric trait must be accurate to a great extent (vi) acceptability which emphasize the willingness of the carriers of the biometric traits to willingly submit themselves for a seamless data capture (vii) circumvention which make sure that the biometric trait is not susceptible to imitation in case of fraudulent attacks against the recognition system.

Mostly, biometric traits can be categorized into physical, behavioral, and chemical categories (Arigbabu, Ahmad, Adnan & Yussof, 2015). Physical biometric traits include hand and earlobe geometry, fingerprint, palmprint, face, iris and retina. Behavioral biometric traits include handwriting, signatures, gait and voice waveform. Chemical biometric traits measure user's body properties like body smell or odour, blood glucose, DNA and Electrocardiogram (ECG). Most chemical biometric traits except DNA are not stable in all conditions and situations; hence, they are not dependable and are rarely used (Barkhoda, Akhlaqian, Amiri & Nouroozzadeh, 2011). A summary of these traits is shown in Figure 1.

Primarily, biometric systems work by extracting features from the acquired biometric traits of an individual. These features are used to form a feature template stored in a database for identification and verification purposes, which are the two major modes of operation of any biometric system (Lumini & Nanni, 2017). Identification is a one to many mode of biometric comparison. It entails comparing the features extracted from the captured biometric trait (query traits) of a person with all the feature templates (stored traits) stored in a database. This is done

in order to determine a person's identity or find a single individual out of multitude whose biometric traits have been previously stored in the database. On the contrary, verification is a one to one mode of biometric comparison. It entails comparing the features extracted from the captured biometric trait of a person with the feature template of the same individual stored in a database. This is done to authenticate or further establish the claim of identity made by a person. The result of both biometric modes could either be genuine/accept or impostor/reject.

4.2 Ocular Biometrics

This branch of biometrics uses the unique physiological characteristics of the eye region to identify an individual (Nigam et al., 2015). It has attracted considerable attention of researchers in the past decade due to the fact that the region possesses the most accurate, highly reliable, well protected, stable and almost impossible to forge biometric signatures (Frucci et al., 2016). Their stability as an internally protected, yet externally visible organ of the eye is also of a great advantage (Yin et al., 2015). Biometric traits in this region as shown in Figure 2 include cornea, lens, optic nerve, retina, pupil, sclera and iris.

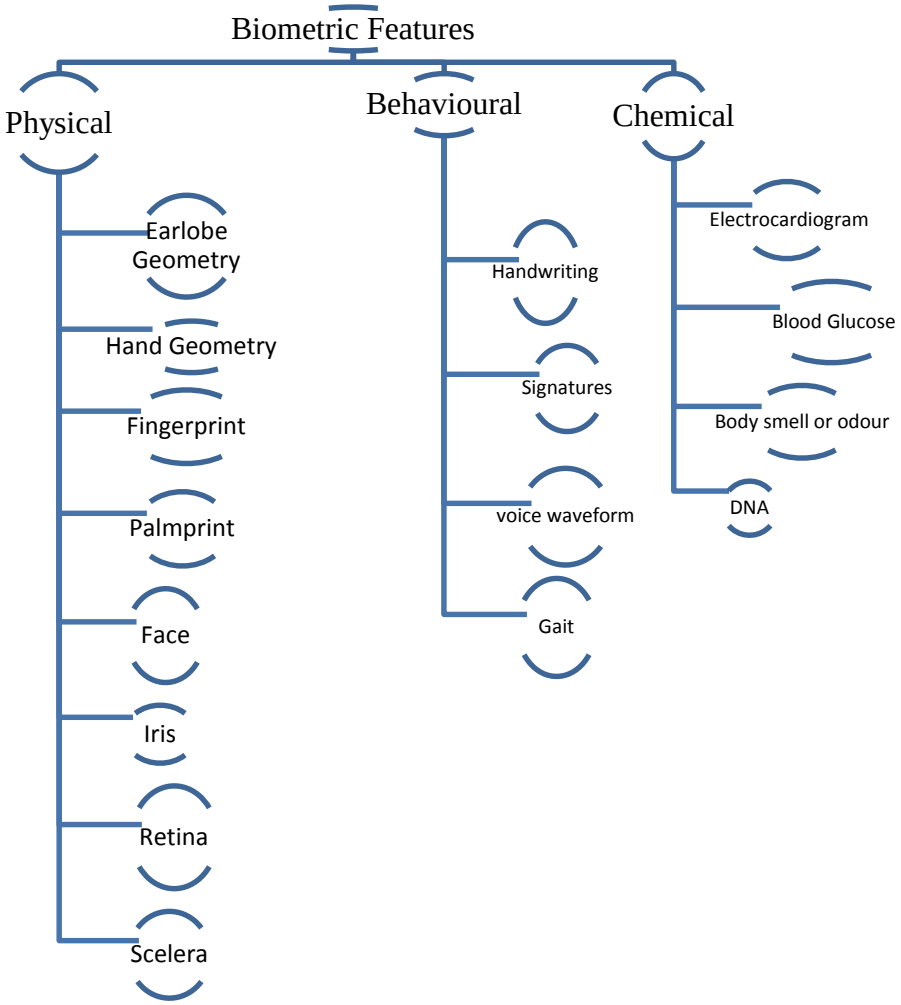

Figure 1: Overview of Biometric Traits

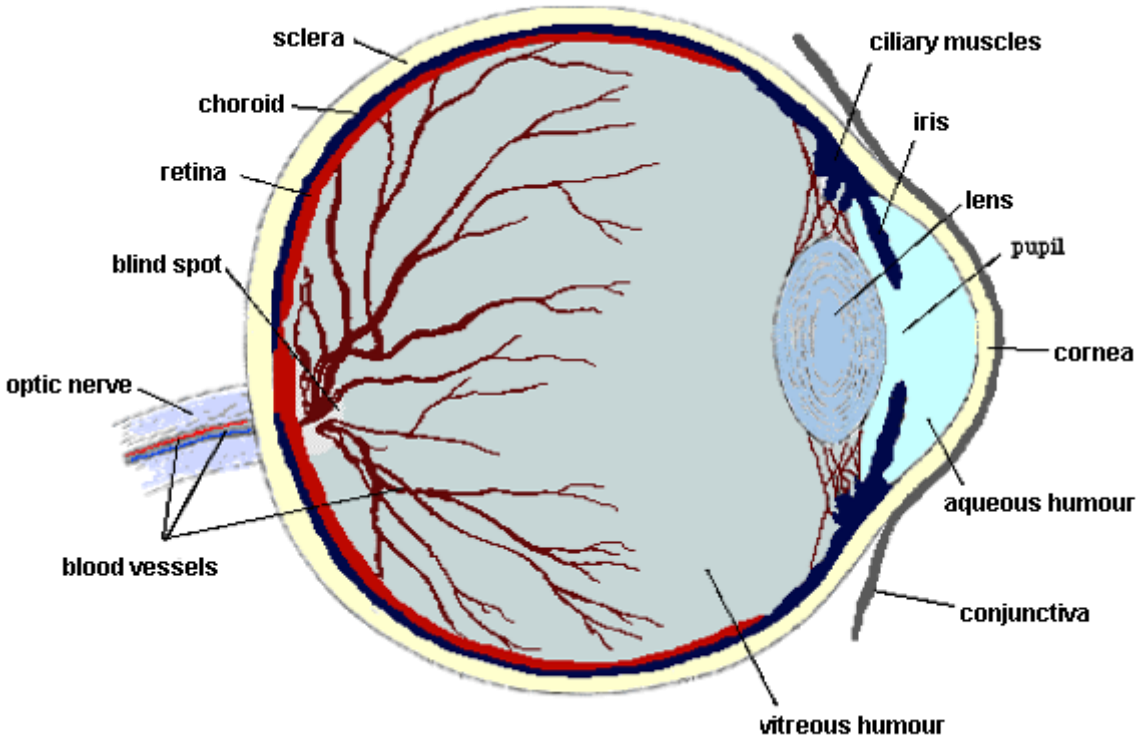

Figure 2: Structure of the Human Eye (Joan, 2017).

Of all these traits, iris which is a thin coloured and circular structure in the eye is the most investigated and widely known (De Marsico et al., 2016) while the retina is the most secured (Jagadiswary & Saraswady, 2016).

Although both iris and retina belong to the same region of the eye, they utilize different imaging procedures. Since iris is located in front of the eye, its acquisition process using a near infra-red or invisible wavelength light is nonintrusive. However, this has made it susceptible to being easily forged. High-quality photograph of iris images captured at a distance of few centimeters to meters and even on motion have been reported to be used in developing synthetic images that have been used to spoof an iris recognition system (Unar et al., 2014). Furthermore, iris pattern can be printed on contact lens and can be used to deceive an iris recognition system (Lefohn, Budge & Shirley, 2003) while multilayered and three-dimensional artificial irises

have been reported to be used in spoofing a biometric sensor (Lefohn et al., 2003; Nixon et al., 2008; Sabarigiri & Suganyadevi, 2014).

On the contrary, retina as shown in Figures 2 and 3 is the light-sensitive thin layer of complex blood vessels and nerve cells located at the posterior region of the eye. It has a well-structured pattern of blood vessels which are unique in individuals. Studies have revealed that these patterns are unique even in identical twins as they are not genetically determined (Sadikoglu & Uzelaltinbulat, 2016; Waheed et al., 2016). Due to the richness of the blood vessel pattern on the retina, it is possible to obtain 400 unique data points from the retina, as opposed to around 200 unique data points available in the iris (Nigam et al., 2015). Furthermore, retina recognition has the best error rate of 1 in 10,000,000 compared to iris recognition of 1 in 131,000, fingerprint of 1 in 500+, speaker recognition of 1 in 50 and hand geometry of 1 in 500 (Cofta & Lacohée, 2008; Dunker, 2003).

However, studies carried out have shown that though the retinal vascular structure can be altered by diseases, the typical retina remains stable throughout a person's lifetime (Isabel et al., 2016) and a retina based recognition system is the most stable and accurate biometric system (Waheed et al., 2016). Furthermore, the retina remains the only biometric feature that has not been forged (Frucci et al., 2016). Hence, retina satisfies most characteristics required of a biometric trait. However, its location at the back of the eye ball has made its acquisition procedure using an infra-red fundus camera an intrusive and tedious task as it requires a special set up and maximum level of cooperation from the users (De Marsico et al., 2016; Jagadiswary & Saraswady, 2016). This has prevented it from gaining wide acceptance and has limited its usage to high security applications.

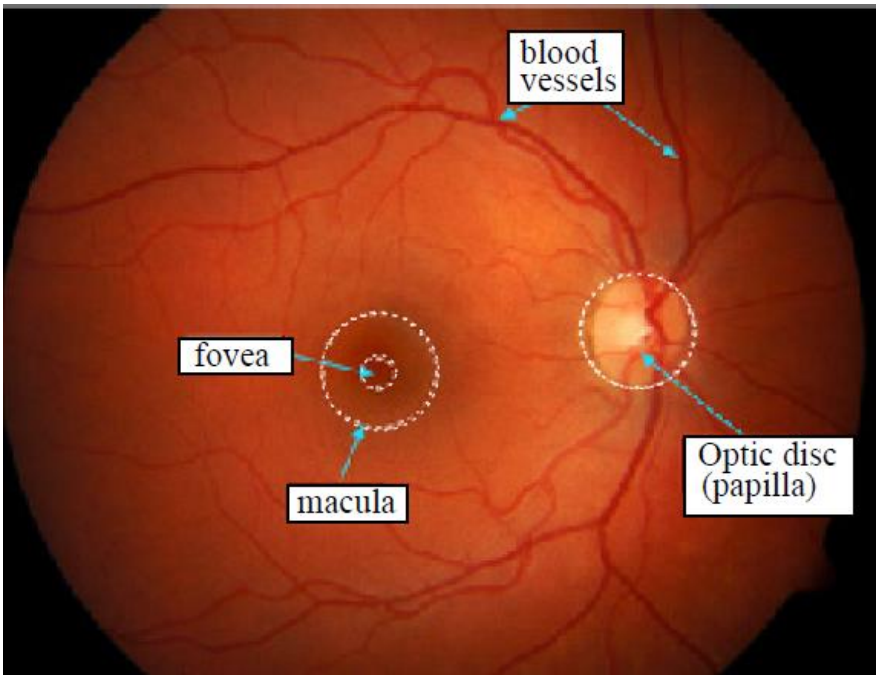

Figure 3: Healthy Retinal Image (Kauppi, Kalesnykiene, Kamarainen, Lensu, & Sorri, 2006)

a) Diabetes Retinopathy and the Human Retina

An average of 387 million people worldwide are afflicted with diabetes, of this large number, 22 million are in sub-Saharan Africa with Nigeria (being the most populated country in Africa) hosting 4 million people with diabetes (Fasanmade & Dagogo-Jack, 2015). DR has been diagnosed to be a micro vascular complication of diabetes (Hendrick et al., 2015) with approximately 10% of its patients suffering from DR (Yin et al., 2015). It is estimated by World Diabetes Foundation (WDF) that over 439 million people will be suffering from diabetes by 2030 (Kaur & Mittal, 2018; Liu et al., 2017), of these, 300 million will have diabetic retinopathy by 2025 (Adalarasan & Malathi, 2018). Complications of DR are seen in the disorder of the retinal vasculature that results in a progressive damage to the retinal blood vessels which could eventually lead to a partial or total loss of vision and blindness (Filiberto, Amin and Julie, 2018; Kusakunniran, Wu, Ritthipravat, & Zhang, 2018).

The presence of DR could also lead to changes in blood vessel structure and vessel distribution which in turn could results to new vessel growth (Franklin & Rajan, 2014). Also, changes in the blood vessel diameter are direct indicators of retinal vasculature abnormality (Abbadi & Saadi, 2014). Furthermore, retinal infected by DR shows signs of lesions such as micro aneurysms, cotton wool spots, exudates, macular edema, and hemorrhages (Sidibé et al., 2015). All these symptoms of DR as seen in retinal images could have adverse effects on the recognition accuracy of retina recognition systems (Amin, Sharif, Yasmin, Ali & Fernandes, 2017; Sadikoglu & Uzelaltinbulat, 2016; Waheed et al., 2016).

Generally, the symptoms of DR are classified into Non-Proliferative Diabetic Retinopathy (NPDR) and Proliferative Diabetic Retinopathy (PDR) (Senapati, Swain, & Prasad, 2016; Amin et al., 2017; Nakao, Yoshida, & Sonoda, 2018) The first stage of DR infection is called the NPDR stage; it occurs when blood vessels become damaged, swollen and blood into the retina. It is characterized by the presence of lesions majorly Micro Aneurysms (MAs), haemorrhages, soft and hard exudates. Depending on the position and amount of these lesions, NPDR stages can be categorized into mild, moderate and severe NPDR as shown in Figure 4 (Senapati et al., 2016; Slean & Khurana, 2018; Adalarasan & Malathi, 2018).

The mild NPDR stage; being the early stage of NPDR and the first visible signs are characterized by the presence of MAs. They are reddish in colour, smaller in size with a circular shape and occur as a result of leakage of blood from tiny blood vessels of the retina (Usman, Khalid, Tariq, Khan & Azam, 2014). In addition to the presence of MAs, when bloods filled with lipids and proteins are leaked or spilled from the damaged blood vessels into the surface of the retina, yellowish spots called exudates are seen; this signifies the moderate NPDR stage (Altomare, Kherani, & Lovshin, 2018). Finally, the increase in the number of exudates coupled with the rupturing of the walls of MAs yielding bright red dots known as haemorrhages signifies the beginning of the severe stage of NPDR.

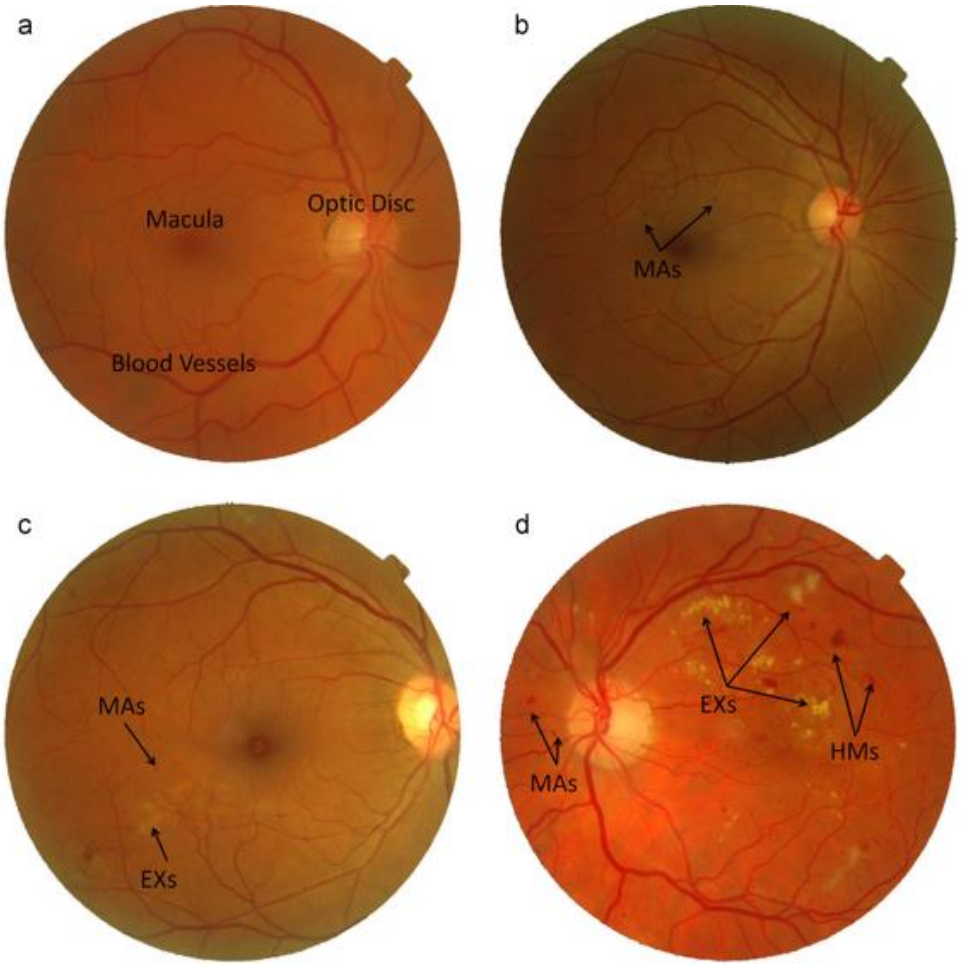

Figure 4: Retina and NPDR Stages.

a) Healthy Retinal Image b) Retina with Mild NPDR c) Retina with Moderate NPDR d) Retina with Severe NPDR (Usman et al., 2014)

The second stage of DR is called PDR; this is the advanced stage that is characterized by the prevention of blood flow in the vessels (Senapati et al., 2016) and the growth of new abnormal blood vessels in different regions of the retina (Amin, Sharif & Yasmin, 2016) as shown in Figure 5. PDR causes a more severe loss of vision than NPDR as it can affect both central and peripheral vision. However, both stages can result in total blindness of the eye (Watson, Machen, & Leiderman, 2018).

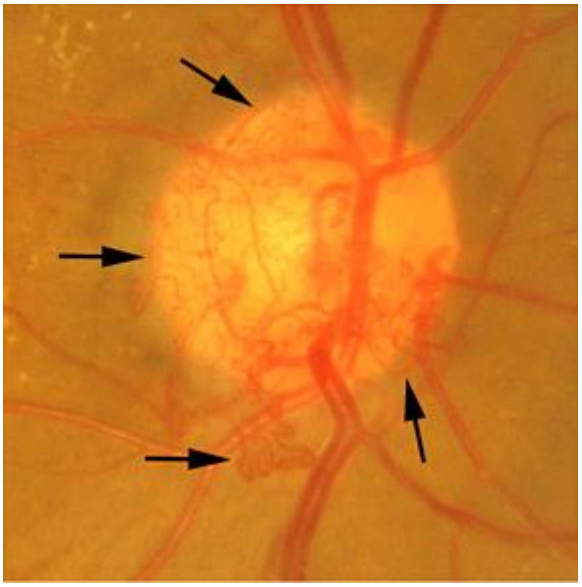

Figure 5: Arrows indicating Growth of New Vessels (Welikala et al., 2015)

4.3 Biometric Recognition Stages

The task of identifying and verifying the identity of an individual using their unique biometric traits is known as biometric recognition. Every biometric recognition approach traverses similar recognition stages as shown in Figure 6. With emphasis on retina recognition, the stages are exhaustively discussed as follows:

a) Image Acquisition Stage

High quality photographs are needed to detect and analyze symptoms of diseases present in images used for medical analysis. However, the fact that retina is small and located at the posterior region of the eye makes its capturing a difficult task when compared to other biometric traits. This has necessitated the need for a special scanning device that requires special set up. Users are expected to position their eyes very close to the lens of the scanning device, and remain stationary focusing on a revolving light being emitted by the scanning device. Any movement by the user at this point can interfere with the capturing process and cause the process to be terminated and restarted (Sadikoglu & Uzelaltinbulat, 2016). Furthermore, users are not expected to wear eye glasses as light reflection from the glass may

bring about interference with the signal of the scanning device (De Marsico et al., 2016). Subject to the level of cooperation of the user, the capturing process can be up to a minute.

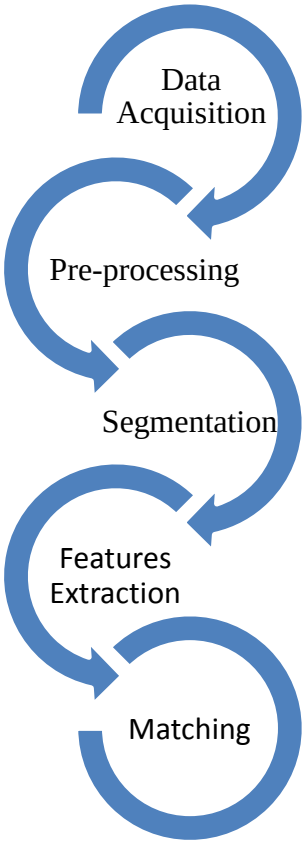

Figure 6: Biometric Recognition Stages

A successful data capturing process produces three to five circular images of the retina which in turn produces a template that is just 96 bytes. This is the smallest of any biometric technologies (Sadikoglu & Uzelaltinbulat, 2016). The most popular and widely used retina scanning device amongst others is the fundus camera. Fundus is a capture of the interior surface of the eye which is opposite the lens containing organs such as the retina, optic disc, macula, fovea, and posterior pole (Mahesh & Kashid, 2013). Digital Fundus Images (DFI) are images of the retina as captured by the fundus camera. DFI could be in any of the following categories as presented by Abràmoff, Garvin & Sonka, 2010; Mahesh and Kashid, 2013; Hendrick et al., 2015; Baumal, 2018.

1. Fundus Photography: this is also called red-free photography. This could be obtained when infrared light from the fundus camera is used to illuminate the blood vessel pattern of the retina. The resulting 2-D representation of the blood vessel pattern is projected onto the imaging plane of the scanning device from the reflected light; this process is termed fundus imaging. This approach can successfully capture the pattern of blood vessels on the retina and any variations of the blood vessels as a result of ocular diseases. To ensure that the best photographs are obtained, the eye of the user must be well dilated, fixation must be on the target; and lids and lashes must be held widely opened. The major limitation of this approach is that it produces only 2-D representation of the 3-D semi-transparent retinal tissues projected onto the imaging plane.

2. Color Fundus Photography: To capture a coloured retinal image, a colour fundus camera whose sensor has high spectral sensitivity will be needed. This will be used to capture the coloured image of the retina along their different Red (R), Green (G), and Blue (B) spectral wavebands. For fusion purposes along spectra wavebands, certain filters and gray-level camera can be used to capture any RGB wavelengths of interest. A popular approach is to use a red filter for getting wavelengths of red colour and register the filtered light using a gray-level camera. A Zeiss 300 or Topcon 35° fundus photograph cameras with magnification of 2.5x to 3x supported with Kodachrome or Ektachrome color slide film can be used for Color fundus photography. Due to these requirements, a colour fundus camera is very expensive and not widely used.

3. Stereo Fundus Photography: This approach creates two images of the same subject taken from two positions—that of the photographer's left eye and that of the photographer's right eye. This yields different view angles of the retina for depth resolution. This approach of photography is suitable for capturing the 3-D shape of the retina.

4. Hyper Spectral Imaging: this is an improvement to colour fundus photography, it entails capturing the multiple specific wavelength bands of the reflected light from the retina. A modified commercial fundus camera, a liquid crystal tunable filter and a low-noise CCD detector can be used for this purpose; they could easily capture sequential hyper spectral images of the human retina and the metabolic status of the retina. The technique allows wavelength-specific visualization of retinal lesions that may not be visible using a white light source camera. The technique may facilitate localization of retinal and disc pathology and consequently facilitate the diagnosis and management of retinal disease such as glaucoma, diabetes retinopathy, hypertensive retinopathy etc.

5. Scanning Laser Ophthalmoscopy: this technique uses time sequence to capture a single wavelength laser light reflected by the retina. It utilizes horizontal and vertical scanning mirrors to scan a specific region of the retina and create raster images viewable on a television monitor. Unlike conventional photography, which obtains two-dimensional imaging, scanning laser techniques utilize confocal imaging methods to obtain high-resolution images both perpendiculars (x-axis, y-axis) to optic axis and along the optic axis (z-axis). Due to this technique, ability to capture the image of the retina with a high degree of spatial sensitivity is possible.

Summarily, fundus cameras provide good-quality images, however, they are huge, not mobile, expert dependent, and expensive which makes its affordability an issue of concern (Panwar et al., 2015). Also, DFI are characterized by a very low contrast between the retinal vascular patterns and its background (Gupta & Chhikara, 2018). Also, illumination is often uneven or non-uniform which results to the presence of local luminosity and contrast variability in the acquired images (Zhang, Huang, Ji & Xie, 2011). These unwanted artifacts and information yields a low quality image and also make visualization and analysis of blood vessels difficult especially in the presence of pathological signs. Therefore, to obtain a high quality image

suitable for effective visualization and medical analysis, the acquired DFI must be preprocessed.

b) Image Pre-Processing Stage

Image pre-processing task is one of the tasks that must be carefully and meticulously carried out prior to other stages of retina recognition especially the segmentation task of retinal vasculature. Due to the invasive nature of the capturing procedure, instances where users do not fully cooperate for proper data capturing may be experienced. Users may have tears covering their eyes which could blur the view of the retina. Also, some users may find it difficult to hold their eye still during the imaging process therefore causing the retinal images to be unevenly illuminated whereby some sections of the image becomes brighter or darker or in worst scenario some sections become washed out with a significant or total loss of contrast; this is called shading (Tian-Swee, Ameen, Hazabah, Yan-Chai & Chong-Keat, 2015). This unwanted information in images leads to the distortion of its pixels; preprocessing task helps to obtain a high quality image that has a uniform pixel distribution.

As reported by , preprocessing needs to be carried out to achieve the followings: (Frucci, Riccio, Sanniti, & Serino, 2018; Keane & Sadda, 2014; Prentašić & Lončarić, 2016; L. Wang et al., 2016)

1. Noise removal and contrast improvement.
2. Undesired information suppression and desired information preservation.
3. Image enhancement.
4. Intra and inter-image variation mitigation.
5. Increasing the fine details of retinal image data.
6. Improvement of signal-to-noise rate of the retinal image.

Intra-image variations are as a result of the differences in light diffusion, fundus reflectivity and fundus thickness while inter-image variability is due to differences in cameras, illumination, acquisition angle and retinal pigmentation.

Preprocessing techniques employed in literature include contrast enhancement, illumination normalization, mask generation, histogram equalization, contrast limited adaptive histogram equalization, wavelet transform, random transform, bias reduction, image filtering and mahalanobis distance. However, the best approach to contrast enhancement is to use images obtained from fluorescein angiography. In this approach, a yellow dye (fluorescein) is injected into the user's body to enhance the retina vasculature and choroid during photography (Baumal, 2018). Though research has revealed that this approach is effective, yet, it has some negative side effects such as severe seizure attack, myocardial infarction and anaphylactic attacks (Kwan, Barry, Franzco & Franzco, 2006).

Contrast enhancement mainly focuses on the spatial domain of the retinal image while histogram equalization is majorly used to enhance the image contrast. However, histogram equalization has been revealed to be inappropriate for preprocessing retinal images as it does not preserve the brightness of the image but tends to over-enhance the image by increasing its brightness (Tian-Swee et al., 2015). As a result of this, a modification of histogram equalization; Contrast Limited Adaptive Histogram Equalization (CLAHE) was introduced (Kumar & Rana, 2016). This entails partitioning the image into regions then applying histogram equalization to each region. This in turn, allots the intensity values across the entire gray value range thereby making hidden features more visible. However, histogram equalization and CLAHE techniques creates artifacts which are not desirable in the enhanced image (Kumar & Rana, 2016; Tian-Swee et al., 2015).

Complex background could also contribute to an increase in noise in an image (Abbadi & Saadi, 2014). This was further corroborated in the results of the comparative analysis carried

out among histogram equalization, mahalanobis distance and CLAHE by Rahim, Ibrahim, Zaki and Hussain, (2014). The result revealed that using mahalanobis distance approach to separate the background image pixels from the foreground image pixels prior to using CLAHE yielded the best preprocessing result. Mahalanobis distance preprocessing approach capitalizes on the fact that enhancing both the background and foreground pixels of an image may over enhance the image and also introduce some unwanted artefacts into the preprocessed image; therefore, it identifies and eliminates the background pixel while enhancing the foreground image only. Therefore, the proposed research initially employed mahalanobis distance to identify and separate background image from foreground image before using CLAHE to enhance the foreground image alone.

c) Segmentation Stage

A retinal image is composed of several components such as optic disc, blood vessels, macula and fovea as shown in Figure 7. The process of separating and analyzing these components for effective features extraction is called segmentation. The component to be separated from others depends on the task at hand. Segmentation task becomes more complicated when the retina is infected with diseases and begins to show pathological signs (Zhang et al., 2014).

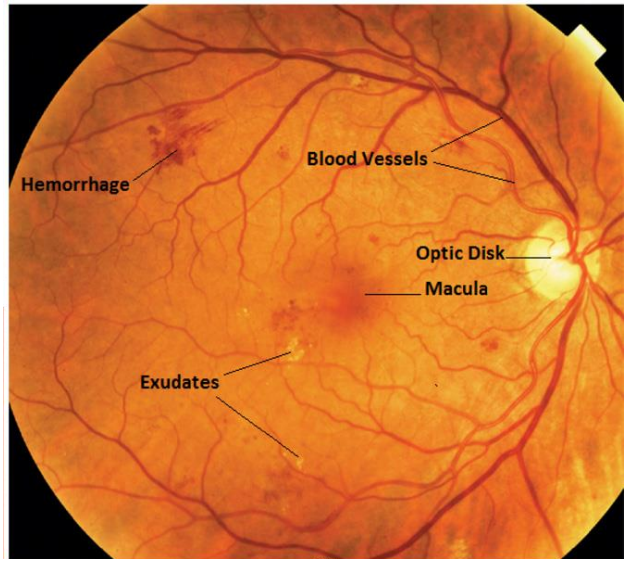

Figure 7: Anatomical Structures in the Retina (Imani & Pourreza, 2016)

In this research, components of healthy retina images will not be segmented since they have clean components. However, segmentation task in retinal images with symptoms of DR cannot but encompass the detection and separation of blood vessels and lesions from other components of the retina. Therefore, this research will consider the segmentation of both blood vessels and exudates in diabetic retinal images.

i. Blood Vessels Segmentation

The segmentation and inspection of retinal blood vessel features such as diameter, illumination, tortuosity and optic disk morphology as shown in Figure 8 have been revealed to be crucial structural indicators for evaluating the presence and stage of diseases including DR (Tian-Swee et al., 2015). However, this could be a difficult task due to the presence of pathological signs in form of holes and bunch in the retinal vascular map causing abnormal structures and growths in the blood vessels. This could further result in the production of false blood vessels and eventually high false recognition rate (Waheed et al., 2016). According to literature, blood vessels segmentation methodologies can be broadly classified into rule and pattern recognition based methodologies (Frucci et al., 2016; Geetharamani & Balasubramanian, 2016).

Rule based methodologies are unsupervised segmentation techniques that make use of mathematical morphology, adaptive thresholding, vessel tracking, multi-scale analysis, matched filtering and model-based algorithms in segmenting retina blood vessels. Pattern recognition based methodologies are supervised segmentation techniques that make use of Gaussian and its derivatives, Gabor wavelet transform, artificial neural network, back-propagation network, multi-layer perceptron, K-nearest neighbors, support vector machines and random forest. for building classification models needed to group retinal image pixels as either vessel or non-vessel pixels. Conversely, pattern recognition based techniques require data whose blood vessels are manually labeled as vessels or non-vessel pixels for the purpose of training the model that will be used for segmentation.

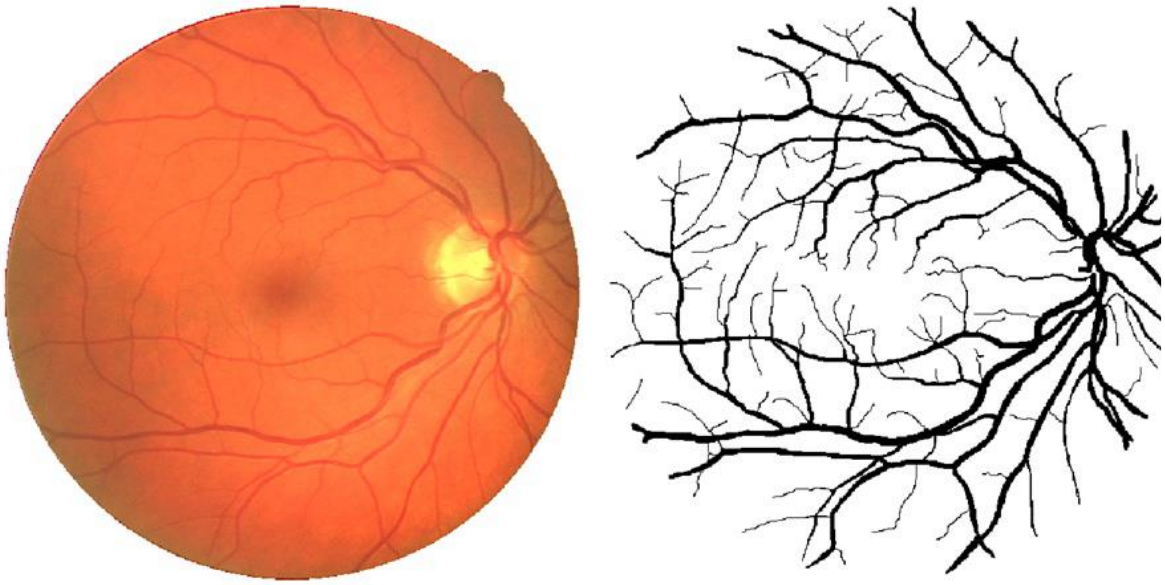

Figure 8: Blood Vessels Segmentation from a Retina (Waheed et al., 2016)

Rule based methodologies attempt to find inherent patterns of blood vessels in retinal images that can be further used to determine if an individual pixel is a vessel or non-vessel pixel. Therefore, manually labeled data and training time are not needed in rule based methodologies. Summarily, to a great extent, the segmentation methodology to be adopted is a function of the data at hand. Since blood vessels are elongated structures in the retinal image, multi-scale line detectors technique was employed for blood vessel segmentation by Nguyen, Bhuiyan, Park & Ramamohanarao, (2013). This entails varying the length of the aligned lines of the blood vessels at different scales as obtained by the basic line detector. This was done to capture blood vessels of different lengths. The varied lengths are then linearly combined to produce the final segmented blood vessels. The drawback of the proposed method is that false blood vessels can be detected around the Optic Disk and pathological regions such as dark and bright lesions.

Region growing method with automatic seed point selection was used to extract blood vessel network from retinal images by Karunanayake & Kodikara, (2015). This entails dividing the retina pixels into 100 × 100 pixel blocks in order to apply region growing segmentation method on block basis. Automatic seed placement method was used to determine the segmentation

starting point (seed point) due to the intensity variation of the pixels of the pertinent block. The region is then iteratively grown by comparing all unallocated neighboring pixels. However, their approach could successfully capture thick blood vessels but failed to capture thin blood vessels.

Due to the limitations experienced when single algorithms were used, two or more algorithms are being hybridized for a better segmentation task. Such was employed by Mapayi, Tapamo, Viriri & Adio, (2016). A combination of difference image and k-means clustering were employed for blood vessels segmentation. Stationary points in the blood vessel center lines were used to model and detect twists in the blood vessel segments. Afterwards, arc chord ratio was combined with the stationary points so as to compute the tortuosity index (the measure of twists and curvature) of the blood vessel. The approach yielded appreciable segmentation in terms of sensitivity and accuracy but it only focused on thick blood vessels whereas, both thick and thin blood vessels are properties of interest when segmenting infected retinal images.

Hessian-based multi-scale filtering and optimized parameters acquired through genetic algorithm was employed to segment wide blood vessels by Rodrigues & Marengoni, (2017). Furthermore, line detector for curvilinear structures in 2D was used to segment the winding lines that are 1-pixel wide. The outcomes of the two methods were later merged with Dijkstra's single-source shortest path algorithm for both wide and 1-pixel thin blood vessels. The experimental results of the approach achieved an average accuracy of 0.9465.

Convolutional Neural Network (CNN) and Random Forest (RF) were as well used for blood vessels segmentation by Wang et al., (2015). In their research, CNN was used as trainable hierarchical blood vessel segmentation while RF was used as the vessel classifier. The hierarchical features extracted from the intermediate and last layer outputs of CNN were fed into the RF classifier for training. After which ensemble method of winner-takes-all was used

to predict whether a pixel belongs to a blood vessel or not. Though their approach addressed the presence of pathological signs, it however, wrongly segmented high light regions. Also, the pixels of optic disc are falsely segmented as vessel and two parallel blood vessels with short distance were classified as one (Zhu et al., 2017).

An integrated approach which uses Dempster–Shafer edge detector for retinal blood vessels detection and diameter measurement was carried out by Li & Wee, (2014). The technique merged the strengths of Laplacian of Gaussian (LoG) and canny edge filters in determining vessels and its path in an input retinal image. However, canny filter is more sensitive for edge detection in noisy environments but its vessel detection is characterized by many broken edges which results to loss of some boundary information. In contrast, a LoG filter can create more continuous edges when compared to a canny filter thereby resulting to a more consistent detection results. The performance evaluation of the approach on public retina databases yielded 100% vessel detection rate for large vessels and 89.9% for small vessels, also, 5% error rate on vessel diameter measurement was achieved.

Since literature have revealed that the impact of DR on retina is seen in changes in retinal blood vessels, these changes can be effectively determined when the blood vessels are accurately segmented and the changes in them are effectively captured, hence, Dempster–Shafer edge detector will be adopted in this research.

ii. Optic Disk Localization and Exudates Segmentation

Locating the Optic Disk (OD) and their eventual removal (as the case may be) is a crucial step in diagnosing several diseases of the eye; diabetic retinopathy inclusive (Reza, 2018). Besides the exudates, OD is the only area in the retina that has similar brightness, intensities and color range (Joshi & Karule, 2018; Kusakunniran et al., 2018). Therefore, to facilitate exudate segmentation OD must be detected and expunged from the retinal image (Panda & Panda,

2017). However, OD is round in shape and larger in size when compared to exudates. This connotes that difference in size and shape of OD and exudates could be used to distinguish them.

An example is seen in OD localization and exudates detection technique proposed by Amin et al., (2017). The technique identified and removed OD from retinal image using a hybrid of statistical and geometrical features set generation. Afterwards, four different classification families: probabilistic, geometric, K Nearest Neighbor (KNN) and tree-based technique were used to classify the features set as either exudates or non-exudates. The performance of five probabilistic based classifiers such as Naive Bayes, Bayesian net, Naive Bayes updateable, Bayesian logistic regression and multinomial naive Bayes were verified. For the geometric family, performance of four variants of SVM such as linear, quadratic, cubic and Gaussian kernel functions were verified. Fine, medium and weighted are the three KNN classifiers used while ensemble bagged tree classifier was used to represent the tree-based family.

Comparative analysis of the classifiers was carried out on eight retina dataset using accuracy and area under curve. Of the geometric family, Gaussian has 98.9% accuracy while Bayesian logistic regression and naive Bayes updateable showed 100% accuracy for the probabilistic families. Among the tree-based classifiers, ensemble bagged tree classifier produced 100% accuracy for most of the datasets while weighted showed an average of 96% accuracy for all the datasets.

In the same vein, size of bright regions, intensity, vessel direction and OD edges were the extracted features used to determine OD location by Xiong & Li, 2016. Afterwards, a confidence score of the extracted features were computed. The pixels with the highest confidence scores are the expected OD region. Performance evaluation of the approach was carried out using DRIVE, STARE, DIARETDB0 and DIARETDB1 public retinal databases. An accuracy of 100%, 95.8%, 99.2%, 97.8% were recorded when DRIVE, STARE,

DIARETDB0 and DIARETDB1 public retinal databases were used to evaluate the performance of the technique.

Furthermore, literature have revealed that blood vessels and optic nerves enters the retina through the OD, therefore, blood vessels can be tracked from the rim of the OD (Xiong & Li, 2016). Such approach was employed by Sangita, (2017). Equiripple low pass finite impulse response (FIR) filter was designed to suppress the blood vessels that dominated the retinal image so as to enhance the OD region. Afterwards, grayscale morphological dilation was employed to segment the OD region. Public retinal databases such as DRIVE, DIRATEDB0, DIRATEDB1 and DRIONS were used to evaluate the proposed approach. Accuracies of 100%, 96.92%, 98.98% and 100% were recorded with sensitivity and specificity in the range of 74.60–87.07%, 99.39–99.61% respectively.

An optic disk localization method using vessel symmetry line was proposed by Panda & Panda, (2017). The approach entails dividing the blood vessel into two similar halves using vessel symmetry line, afterwards, the initial OD center was computed using the highest vessel component count. Finally, OD center was determined using iterative center of mass computation. An average of 99.49% OD detection accuracy was recorded when 10 public retinal databases were used to evaluate the proposed approach.

Rodrigues & Marengoni, (2017b) also proposed an optic disc and blood vessels segmentation approach using mathematical morphology, wavelets, and Hessian-based multi-scale filtering. A total of 20 retinal images obtained from DRIVE database were used to evaluate the approach. Of these, OD of 19 retinal images were accurately localized.

Furthermore, a combination of mean shift algorithm and normalized graph cut algorithm were used for exudates extraction by Banerjee & Kayal, (2016). Prior to this, optic disk boundary was detected and subsequently removed. Thereafter, mean shift algorithm was used to segment

the input retinal image which were labeled and represented as nodes in a graph. The result obtained was used as an input to the normalized cut algorithm for clustering. When only mean shift algorithm was used, two false negative regions were recorded; however, this drawback was overcome when the output image of the mean shift algorithm was used as input into the normalized cut algorithm.

A novel approach to retinal exudates extraction based on Morphological Component Analysis (MCA) algorithm was proposed by Imani & Pourreza, (2016). Their approach entails primarily separating blood vessels from other components in a retinal image so as to facilitate exudate detection. Afterwards, dynamic thresholding algorithm was used to create initial exudates map while morphological operators were used to detect the exact exudates border in the separated lesion part of the retinal image. Experimental results carried out on three public datasets demonstrated that the approach achieved satisfactory results, however, it was discovered that some parts of the lesions may not be completely separated.

Conclusively, a hybrid Gaussian Mixture Model (GMM) and Support Vector Machines (SVM) classifiers were used for exudates segmentation in retinal images by Akram et al., (2014). GMM has the capability to accurately represent data distributions and also caters for overlapping patterns while SVM caters for data that is well separable by a decision boundary and has good classification cum rapid training phase. Their approach entails creating a binary map of candidate regions using filter bank after which a detailed feature set was created for each candidate region based on the properties of the exudates. The hybrid GMM-SVM classifier based on a weighted probabilistic ensemble was now used to classify the region as exudates region or non-exudates region. The evaluation of their approach achieved high sensitivity, specificity and accuracy.

Edge distance seeded region growing method will be used to identify different lesions in the retinal image while hybrid GMM-SVM will be used to classify the image pixels into exudates and non- exudates pixels.

d) Features Extraction in Retinal images

Features extraction is another important stage in every biometric recognition system as its success will go a long way to determine the output of the next phase (matching/classification phase) and the eventual accuracy of the recognition system (Panda, Puhan & Panda, 2016). It is the process of generating unique features from the acquired biometric traits. These features are further used to form a feature vector which makes up a feature template to be stored in a database for recognition purposes. According to Kaur & Mittal, (2018), features extraction in retinal images could be image or lesion based. Image based approach extracts features from the entire image regardless of the presence of pathological signs or not. This approach is perfect for healthy retinal images which are believed to have clean components by default. On the contrary, lesion based approach extract features from the retinal images taking into consideration the presence of pathological signs. Therefore, this approach is suitable for unhealthy retinal images. Image based features include the structural components of the retinal images such as the structure, contrast and luminance features that could be mathematically computed from the entire image. However, lesion based features include region, morphological, region, intensity and structural based features.

Due to the richness of the retinal blood vessel pattern, it is possible to obtain 400 unique data points from the retina (Nigam et al., 2015). Blood vessel features could be grouped into morphological and intensity based features. Morphological features include blood vessel length, lines, width, tortuosity or branching patterns, branching angles, ridges, maximum principal curvature, number of vessel pixels, vessel segments, vessel orientations and density, number and locations of vessel's end points, bifurcation and crossover points.

On the other hand, intensity based features are features extracted from the spectra bands (RGB) of coloured retinal images. In this approach, features are majorly extracted from the green channel as literature have revealed that the channel exhibits the best vessel cum background contrast in retina images while the red channel has the lowest contrast and the blue channel has a very small dynamic range (Wang et al., 2015; Imani & Pourreza, 2016; Zhu et al., 2017). Intensity based features can be measured in terms of Max Intensity, Min Intensity, and Mean Intensity (Waheed et al., 2016).

Several methodologies have been employed by researchers in extracting features of interest from retinal images. Ten features were extracted for exudates detection in diabetic retinal images by Akram et al., (2014) using wilcoxon rank sum and Ansari–Bradley statistical techniques. Also, four main descriptors: shape, color, intensity and statistical feature were used for exudates detection by Akram et al., (2014). Similarly, statistical techniques were used for feature extraction by Welikala et al., (2015). Features extracted include number of vessel pixels, vessel segments, vessel orientations and vessel density.

Furthermore, an n-dimension feature extraction approach was implemented by Zhu et al., (2017). Five different categories of features such as twenty-nine local features, six morphological features, two Hessian features, phase congruency and divergence of vector field were extracted from the green channel of the retinal image. The first and second order derivatives of 2-D Gaussian filtering were used to extract the local features while top and bottom-hat transforms were used to extract the morphological features. Statistical techniques were then used to compute phase congruency, hessian feature and divergence of the vector field. Moreover, connected component analysis was used by Waheed et al., (2015) to extract candidate regions from diabetic retinal images. Thereafter, seven different features based on the morphological properties and intensity values of true and false vessels were extracted.

Eight newly constructed descriptive statistical features formed from statistical moments were introduced by Barkana, Saricicek & Yildirim, (2017). Mean and median measurements of image pixels' intensity values were carried out in horizontal, vertical, up-diagonal, and down-diagonal directions. The features were further used for classification by three algorithms and the results obtained revealed that the descriptive statistical features can be employed in retinal vessel segmentation as well as supervised classification.

Geometrical shape features including four boundary based features and seven lesion based features were extracted from blood vessel patterns by Pouya & Pourghassem, (2017), though, only regions surrounded by thick blood vessels were considered. However, Waheed et al., (2016) extracted three morphological features and eleven discriminating features including bifurcations and ending points from segmented true and false blood vessels of the retinal image using windowing crossing number technique.

In this research, three categories of features were extracted; the first category are structural features such as luminance, contrast and structure which were extracted from the healthy retinal images. The second category of features are the morphological features such as bifurcation points and vessel endings (minutiae), vessel diameters, lines, branch points, ridges end, and bifurcation points which were extracted from the segmented blood vessels of the diabetic retinal images. The third category are lesion based features such as extent, major axis length, filled area, compactness, maximum intensity, mean intensity and energy which were extracted from the exudate region of the diabetic retinal images. Therefore, a total of sixteen features were extracted from both healthy and diabetic retinopathy retinal images.

e) Matching/Classification Phase

The aim of every biometric recognition system is to verify and establish the identity of an individual using their unique biometric traits. This decision is achieved at this stage. Matching

greatly depends on the outputs of the feature extraction phase and the result obtained at this stage has a great impact on the performance of the retinal recognition system (Waheed et al., 2016). It entails comparing the feature vector of a query image with the already saved (enrolled) feature vectors. A match score is obtained after the comparison and a decision module confirms or discards the identity in question based on the match score.

Matching has been reported in the literature to be carried out using different approaches. A matching model was employed by Dehghani, Ghassabi, Moghddam & Moin, (2013). This was achieved by comparing the similarity of selected model functions using the closeness and orientation of the polar coordinates of each image corner points.

An approach proposed by Köse & Ikibaşs, (2011) involves translating, rotating and scaling the query image using varying directions and scales so as to find the maximum pixels of sample lines that matched the enrolled images. Similarity measurements carried out on these sample lines are then compared together. Lajevardi, Arakala, Davis & Horadam, (2013) also put translation, rotation and noise issues into consideration prior to matching, therefore, a combination of graph registration approach and error tolerant graph matching technique was used to attain the best alignment between the two graphs for matching purposes.

In Figueiredo, Kumar, Oliveira, Ramos & Engquist, (2015), weighted norms of function spaces were used to quantify the location and measurement of vascular network. An iterative hierarchical matching structure was introduced by Pouya & Pourghassem, (2017). The technique used step-by-step elimination of candidates searched from the simple to the complex candidate features. The remaining features of the query and enrolled features were then matched in a hierarchical manner. Cosine similarity index matching technique introduced by (Waheed et al., 2016) carried out score based matching which turned out to be efficient for

instances where multiple features are extracted and fused, this approach will be adopted in this research.

4.4 Related Works

Several attempts and methodologies have been reported in the literature towards improving the accuracy of retina recognition systems especially in the presence of DR lesions. Kusakunniran et al., 2018 presented a multilayer perceptron and iterative graph cut technique for exudates extraction in DR retinal images. Multilayer perceptron was used to identify initial seeds of the exudates at high confidence level while iterative graph cut was used to complete the exudate segmentation by clustering the initial seeds. 94 publicly available retinal images available in e-ophtha EX and DIARETDB1 were used to validate the technique and a sensitivity of 0.891 and 0.564 was achieved with e-ophtha EX and DIARETDB1 respectively. Similarly, a technique to identify exudates present in coloured retina images was proposed by Sudeshna & Santi, (2018). Prior to exudates detection, OD was detected and extracted. Afterwards, kernel fuzzy c-means was used to identify and extract the blood vessels while Matched filter alongside Laplacian of Gaussian (LoG) filter were used to extract the exudates. Sensitivity, specificity and accuracy were used to evaluate the performance of the technique. Detailed results are captured in Table 1.

A technique for detecting symptoms of NPDR which are micro-aneurysm, hemorrhages and exudates was proposed by Bouacheria, Benouadah, Cherfa, Cherfa & Belkhamsa, (2018). Top-Hat and morphological gradient algorithm were used to detetand extract the optic disk. Afterwards, blood vessels were extracted using sequential alternate white filter, skeletalization and morphological reconstruction. White top hat algorithm and morphological gradient were then used to detect and remove the exudates from the retina images. the performance of the technique was evaluated using sensitivity, specificity and accuracy. Daniel, Luk´aˇs and Martin, (2017) presented a technique to detect symptoms of DR and age-related macular

degeneration. Prior to symptoms detection, the retina images were enhanced using CLAHE after which Adaptive Gaussian threshold was used to detect the continuous paths of the blood vessels. Subsequently, growing region algorithm was used to identify soft and hard exudates that could be present in the retina image.

Furthermore, Pouya & Pourghassem (2017) extracted geometrical shape features from retinal images using a hierarchical matching structure. These were further used to generate feature vectors used in human identification. Healthy retinal images were used to validate their proposed technique; however, their focus was to reduce the effects of head and eye movements during data acquisition. Similarly, a retina identification system based on neural network was proposed by Sadikoglu & Uzelaltinbulat (2016). The identification system was divided into three phases: image acquisition, computer based processing and features extraction. Back propagation algorithm was used for training the neural network while extracted features of patients suffering from anthemia diseases were used as inputs to the neural networks. Their work reported the prowess of neural network in recognizing retina patterns but does not establish if there is a direct effect of anthemia diseases on retina vascular patterns as not all disease has effect on human retina.

Two methods of feature extraction towards achieving retinal recognition in healthy and unhealthy images were proposed by Waheed et al. (2016). The first method entails extracting structural information from retinal images while the second method extracts minutiae points from retinal images. Both methods were validated using Recognition Rate (RR), False Rejection Rate (FRR), False Acceptance Rate (FAR) and Equal Error Rate (EER) on both healthy and diseased public retinal databases. Results obtained showed that a recognition rate of 100% and 78.57 was achieved for the healthy and diseased retinal images using the first approach while a recognition rate of 92.5% and 85 .57% was achieved for the healthy and diseased retinal images using the second approach. The results revealed that extracting

structural information yields a good result for healthy retinal images while extracting features from blood vessels is acceptable for diseased retinal images. However, the low recognition rate obtained in the second approach may be as a result of few features extracted from the diseased retinal images. No specific disease was their point of focus as the diseased database contains various retinal of individual affected by one disease or the other. Also, the state at which an individual became infected was not considered. An emphasis on a particular diseased would have thrown more light about the effect of such disease instead of generalizing the effects of diseases on retinal.

A retinal verification approach using point set matching was proposed by Ekka, Puhan & Panda, (2015). They are of the opinion that the blood vessels of the optic disc region are more stable and unique, hence, edge map of the optic disc blood vessels were extracted for human verification. With FAR, FRR and EER used as evaluation metrics; a recognition rate of 90.21% was achieved. The blood vessels used for the feature extraction are few and are not sufficient enough to yield robust features extraction. Moreover, only healthy retinal images were considered; hence, the proposed work will not be able to sensitive to the effects of biological disease.

Hussain, Bhuiyan, Mian & Ramamohanarao, (2013) employed multi-scale line detection technique to extract branch and crossover points from retinal blood vessels. Afterwards, geometric Hashing was used to obtain a unique pattern of the extracted branch and crossover points that is invariant to translation, rotation and scaling. A locally gathered coloured retinal images and STAAL retinal dataset were used as test beds. A recognition accuracy of 100% and 95% respectively were achieved.

A retina verification system based on Biometric Graph Matching (BGM) was proposed by Lajevardi et al., (2013). Matched filters in the frequency domain and morphological operators

were used to extract retina vascular structures while BGM was used to compare spatial graphs extracted from the retina vascular structures of two sets of healthy retinal images. Kernel Density Estimation (KDE) was then used to model the distribution of distances obtained from the comparison. If the measured distance is less than or equal to a specified threshold obtained from the model, they are categorized as genuine, otherwise they are labeled as imposter. Single as well as multiple graph measures of the proposed BGM algorithm were considered. With support vector machine as a classifier, 60% of the data were correctly identified for multiple graph measures. False Match Rate (FMR), False Non-Match Rate (FNMR), Equal Error Rate (EER) and Receiver Operating Characteristic were used to evaluate the performance of the proposed method. A recognition rate of 98 % showed that the multiple graph measures performed better than the single graph measure.

Retina based person authentication approach using sparse classifier was proposed by Alexandru, Johannes & Alfred, (2012). Statistical characteristics of the scale-invariant feature transform were extracted from the blood vessels of healthy retinal images. The approach was evaluated using VARIA and DRIVERA public retinal databases. The images in these databases were divided into two so as to study the effect of the approach on smaller and larger datasets. With VARIA, an initial recognition accuracy of 90.71% improved to 99.29% while that of the DRIVERA database improved from 94.64% to 99,295; this showed that the more the images the more the accuracy.

Rotation invariant features based on retinal image moments were extracted from retinal images by Dehghani & Moghaddam, (2011). The proposed approach was without image segmentation and optic disc detection yet high recognition accuracy was recorded. Retinal images from DRIVE and STARE databases were used as test beds. Similarly, retina based human identification method was proposed by Barkhoda, Akhlaqian, Amiri & Nouroozzadeh, (2011). Two feature vectors were extracted from the retinal images using angular and radial

partitioning. This is to eliminate any rotation effects. Fuzzy system was used in the decision-making phase to categorize an individual into an impostor or genuine person. Evaluation of the proposed approach yielded 98.75% recognition accuracy. Healthy retinal images were used as test data while the performance of the approach has not been tested on diseased retinal images.

Moreover, a retinal recognition system using blood vessels energy extracted from the green components of retinal image in a rotation invariant manner was proposed by Rubaiyat, Aich, Toma, Mallik & Rafat-Al-Islam, (2003). Feature matching of the resulting feature vectors was carried out using fast normalized cross-correlation. The performance of the proposed approach was carried out using STARE and DRIVE public databases. A recognition accuracy of 100% and 99.77% respectively was reported. The results, if correct showed that the approach worked perfectly well for healthy retinal images however, what could be the result if it were to be DR images were not considered.

It has been observed that the literature reviewed so far either extract features from healthy or diabetic retinal images with or without employing fusion techniques towards coming up with an improved retinal recognition system. Therefore, the approaches employed could independently recognize healthy or DR infected individual but not both. Also, the works reported so far have not considered the effect of the state of DR infection on retinal recognition system i.e. if the individual became infected before or after data collection. As conjectured in this research, if features extracted from healthy retinal images were used in developing a retinal recognition system; resulting system will be suitable for instances where the individual is healthy likewise if features extracted from diabetic retinal images were used in developing a retinal recognition system; such system will be suitable for instances where the individual has DR. Therefore, this research intends to fill this gap by coming up with a retinal recognition that cannot be limited by the presence of DR lesions in the retinal of the individual before or after data collection. A summary of related literature is provided in Table 1.

Table 1: Summary of Related Works

S/N	Author(s), Year	Retinal Images Considered (Healthy/ Unhealthy)	Lesions Considered	Technique Adopted	Database (Number of Images)	Number of Features Extracted	Performance Evaluation Metrics	Limitations Observed in Relation to the Proposed Research
1.	Kaur and Mittal, (2018)	Healthy/ Unhealthy	Exudates	To determine the presence of exudates, shape and intensity based features were extracted from healthy and unhealthy retinal images using adaptive image quantization and dynamic decision thresholding	Clinical (649) STARE (96) MESSIDOR (400) DIARETDB1 (80) E-Optha EX (82)	Not specified	Mean Sensitivity (88.85) Specificity (96.15) Accuracy (93.46)	The work only focused on the detection and segmentation of exudates in healthy and pathological retinal images. emphasis was not placed on a particular disease.
2.	(Kusakunniran et al., 2018)	Unhealthy	Exudates	Multilayer perceptron and iterative graph cut algorithms were used to detect and extract exudates from DR retinal images	E-ophtha EX (82) DIARETDB1 (89)	Not specified	DIARETDB1: Sensitivity (0.891) E-ophtha EX: Sensitivity (0.564)	The work focused only on exudate segmentation.
3.	Sudeshna and Santi, (2018)	Healthy and Unhealthy	Exudates, Microaneurysm and hemorrhages	Kernel fuzzy c-means was used to identify and extract the blood vessels while Matched filter alongside Laplacian of Gaussian (LoG) filter were used to extract the exudates.	DRIVE (58) STARE (790) DIARETDB1 (902) MESSIDOR (1790)	Not specified	DRIVE Sensitivity 97.11), Specificity (95.71), Accuracy (96.18) STARE Sensitivity (97.62), Specificity(97.81), Accuracy (97.98) DIARETDB1 Sensitivity (96.03), Specificity(94.19), Accuracy (96.51) MESSIDOR (300) Sensitivity (97.78), Specificity(98.03), Accuracy (98.22)	Extracted features were not used to identify the individual

4.	Bouacheria, Benouadah, Cherfa, Cherfa and Belkhamsa, (2018)	Healthy and Unhealthy	Micro-aneurysm, Hemorrhages and Exudates	Blood vessels were extracted using sequential alternate white filter, skeletalization and morphological reconstruction. White top hat algorithm and morphological gradient were then used to detect and remove the exudates from the retina images.	DIARETD1 (50)	Not specified	Sensitivity (97.86) Specificity (99.81), Accuracy (99.75)	Extracted features were used for NPDR grading but recognition was not carried out
5.	Fraz, Jahangir, Zahid, Hamayun, & Barman, (2017)	Unhealthy	Exudates	Morphological reconstruction and Gabor filter were used for candidate exudate extraction. Afterwards lesion based features were extracted from the exudates	DIARETDB1 (63) E-Ophtha Ex (60) HEI-MED (110) Messidor (108)	9	Sensitivity (88.85) Specificity (96.15) Accuracy (93.46) *PPV *FDR *AOC Processing Time	Only DR retinal images were considered and only exudate classification was carried out
6.	Daniel, Luk´aˇs and Martin, (2017)	Unhealthy	Exudates, Microaneurysm and hemorrhages	Retina images were enhanced using CLAHE after which Adaptive Gaussian threshold was used to detect the continuous paths of the blood vessels. Subsequently, growing region algorithm was used to identify soft and hard exudates that could be present in the retina image.	HRFIDB (16) DRIVE(20)	3	HRFIDB (16) Sensitivity(69.81), Specificity(98.76), Accuracy (98.36) DRIVE (20): Sensitivity(63.63) Specificity (99.70) Accuracy (99.7)	A good job was done as emphasis was on symptoms of Diabetic Retinopathy and age-related macular degeneration. THE eventual identification of the individual was not carried out

S/N	Author(s), Year	Retinal Images Considered (Healthy/ Unhealthy)	Lesions Considered	Technique Adopted	Database (Number of Images)	Number of Features Extracted	Performance Evaluation Metrics	Limitations Observed in Relation to the Proposed Research
7.	Pouya & Pourghassem, (2017)	Healthy	None	Geometrical shape features from retinal images using a hierarchical matching structure	STARE(20) DRIVE(40)	11	Accuracy rate (93.73%) and Processing time (0.1124s)	The approach has not been tested on DR images to examine what the recognition accuracy will be as a result of DR lesions
8.	Sadikoglu & Uzelaltinbulat, (2016)	Unhealthy	Not specified	Retinal identification system using backpropagation neural network was proposed	DRIVE (40)	1	recognition rate (97.5)	Their work reported the prowess of neural network in recognizing retina patterns but does not establish if there is a direct effect of anthemia diseases on retina recognition. Features extracted from retinal images of patients suffering from anthemia diseases was used as an input into the adopted Neural network
9.	Waheed et al. (2016).	Healthy/ Unhealthy	Not specified	Structural information were extracted from healthy retinal images while minutiae points (bifurcations and endings) were extracted from unhealthy retinal images	Retina Identification Database (100) and Diseased Image Retina Identification Database (60)	Healthy (3) Unhealthy (2)	Recognition rate Approach I Healthy:100 Diseased: 78.57 Approach II Healthy:92.5 Diseased: 85.57	No specific disease was their point of focus as the diseased database contains various retinal of individual affected by one disease or the other. Also, the state at which an individual became infected was not considered.

	Authors, Year	Retinal images Considered (Healthy/ Unhealthy)	Lesions considered	Technique Adopted	Database (Number of Images)	Number of Features Extracted	Performance Evaluation Metrics	Limitations Observed in Relation to the Proposed Research
10	Bijay, Puhan & Panda, 2015	Healthy	None	Point set matching was used to extract feature map from blood vessels of the optic disk	VARIA (59)	1	FAR, FRR, EER and Recognition rate 90.21	The blood vessels used for the feature extraction are few and are not sufficient enough to yield robust features extraction. Moreover, only healthy retinal images were considered, hence, the proposed work will not be able to be resistive to the effects of biological disease
11.	Lajevardi, Arakala, Davis, & Horadam, (2013)	Healthy	None	Single as well as multiple spatial graphs were extracted from the retina vascular structure of two sets of healthy retinal images	VARIA (233)	2	Recognition rate (98%)	The work could only handle healthy individual and cannot handle occurrence of diseases especially DR
12.	Hussain et al., 2013	Healthy	None	Branch and crossover points that were invariant to translation, rotation and scaling, were extracted from retinal blood vessels using Multi-scale line detection technique.	164 colour retinal images Staal dataset (20)	2	Recognition rate 100% 95% Accuracy	The approach has not been tested on DR images to examine what the recognition rate will be as a result of DR lesions
13.	Alexandru, Johannes, & Alfred, (2012)	Healthy	None	Statistical characteristics of scale-invariant feature transform were extracted from healthy retinal images.	VARIA (233) DRIVERA (280)	2	Recognition rate 99.29% 99.29%	The approach has not been tested on DR images to examine what the recognition rate will be as a result of DR lesions

	Authors, Year	Retinal images Considered (Healthy/ Unhealthy)	Lesions considered	Technique Adopted	Database (Number of Images)	Number of Features Extracted	Performance Evaluation Metrics	Limitations Observed in Relation to the Proposed Research
14.	Barkhoda, Akhlaqian, Amiri, & Nouroozzadeh, (2011).	Healthy	None	Two feature vectors were extracted from the retinal images using angular and radial partitioning.	DRIVE: 40	Blood Vessel Pattern	Recognition accuracy: 98.75%	Healthy retinal images were used as test data while the performance of the approach has not been tested on diseased retinal images.
15.	Dehghani & Moghaddam, (2011)	Healthy	None	Rotation invariant features based on retinal image moments were extracted from retinal images	DRIVE (60) STARE (20)	1	Recognition accuracy: 99.78%.	Only healthy retinal images were used as test data while the performance of the approach has not been tested on diseased retinal images.
16.	Rubaiyat, Aich, Toma, Mallik, & Rafat-Al-Islam, (2003)	Healthy	None	Blood vessels energy extracted from the green components of retinal image in a rotation invariant manner was used for recognition purposes	DRIVE (40) STARE (20)	1	Recognition rate 99,77% 100%	The approach has not been tested on DR images to examine what the recognition rate will be as a result of DR lesions

5. RESEARCH METHODOLOGY

To achieve the set objectives of this research, the following sequential steps were taken:

5.1 Data Collection

With a view to come up with a recognition system that will be able to accommodate the retinal images of a healthy and DR individual, two categories of retinal images were used in training and testing the proposed recognition system. The first category were retinal images of healthy individual. These were acquired from public retina databases such as: Digital Retinal Image for Vessel Extraction (DRIVE) and Structured Analysis of Retina (STARE). The second category were retinal images of DR individual. These were acquired from public retina databases such as Standard Diabetic Retinopathy Database (DIARETDB1) and Diabetic Retinopathy Image Database (DRiDB).

Furthermore, to ascertain if the system will be able to identify the retina of the same individual that were previously healthy but later have DR, retinal images from the same individual were acquired from Clinical Practice Research Datalink (CPRD). CPRD is an electronic health database created in 1987 which currently contains longitudinal primary care records for approximately 13.5 million patients from 601 general practices across the UK of which 5.5 million are currently active.

A cohort study of the research was inaugurated in 2004 to investigate the national prevalence and incidence of diabetic retinopathy in the UK between 2004 to 2014. 7.7 million Patients above 12 years participated in the research. An excerpt of their result containing patients who initially do not have diabetes but later had and those whose diabetes became worse and led to diabetic retinopathy will be used in this research.

5.2 Preprocessing the Retinal Images

In an attempt to make the retinal image suitable for analysis, preprocessing task was carried out to suppress unwanted information while enhancing the needed information. The retinal images acquired were coloured images that are made up of Red (R), Green (G) and Blue (B) components; however, red and blue components are very noisy and have low vessel-background contrast (Wang et al., 2015; Zhu et al., 2017). Therefore, the red and green components of the input image were removed using equation 5 and 6 respectively while the green component that has the best contrast and less noise was retained using equation 7.

$$inp\_img(:,:,1) = 0; \quad (5)$$

$$inp\_img(:,:,3) = 0; \quad (6)$$

$$G(:,:,2) = inp\_img(:,:,2); \quad (7)$$

Furthermore, every coloured image is made up of intensity, hue and saturation information and the most important of these for medical analysis is the intensity (since it shows the effect of varying degrees of light on the acquired retinal images). Hence, the hue and saturation information in the extracted green component were removed using equation 8; this is called gray scale conversion.

$$\mathrm{I} = \mathrm{rgb2gray(RGB)} \quad (8)$$

Where the extracted image intensity is denoted by I.

Furthermore, to enhance the intensity of the extracted green component, mahalanobis distance and CLAHE as proposed by Rahim et al., (2014) were employed to identify and eliminate the background pixel while enhancing the foreground pixels only. In order to achieve this, the mean μ_N and standard deviation σ_N of the statistical distribution of the intensities in input retinal image N were calculated. Thereafter, a sample mean $\widehat{\mu_N}$ and a sample standard deviation $\widehat{\sigma_N}$ were chosen as the estimators for μ_N and σ_N respectively. The intensities of the image

pixel (x, y) tagged $I(x, y)$ were then compared with the mean intensity using equation 9. If $I(x, y)$ is close to μ_N or if d_M is lower than a specified threshold t then the pixel belongs to the background image β, then the foreground image was enhanced.

$$\mathrm{F_{enc}} = \left| \frac{\mathrm{I\,(x,y)} - \hat{\mu}_{\mathrm{N}}}{\hat{\sigma}_{\mathrm{N}}} \right| < \mathrm{t} \tag{9}$$

F_{enc} is the enhanced foreground image.

5.3 Optic Disk Localization and Exudates Detection

In detecting and removing the optic disk, morphological component analysis which operates by varying the intensity of image pixels based on an initial threshold computed was adopted. The algorithm as proposed by Imani & Pourreza (2016) is as follows:

1. Input parameters: input image I_{retina}, the set Φ of optic disk pixels (Φ_{OD}) and exudates pixels (Φ_E), the number of expected iterations denoted by $N_{iteration}$ and the threshold value λ_{vmin}
2. Initialization: set number of sub pixels P = 2, i.e. $\Phi = [\Phi_{OD}, \Phi_E]$, initial optic disk value $OD_v = 0$, initial exudates value $E_v = 0$
3. Compute pseudo sub pixel $P^* = argmax_p \|\Phi_p I_{retina}\|$ where p=1,…,P
4. Set $\lambda_v = \lambda_0 = max_{p \neq P^*} \|\Phi_p I_{retina}\|$
5. iterate $N_{iteration}$ times

   For the optic Disk components:

   i. Update OD_v when E_v is fixed.

   ii. Calculate the pixel residuals r such that $r = I_{retina} - OD_v - E_v$

   iii. Calculate shift invariant shearlet transform Θ_{SIST} of $OD_v + r$ and obtain the coefficient vector α_{OD} such that Θ_{SIST} $(OD_v + r)$

   iv. Hard threshold α_S with λ_v to obtain $\widetilde{\alpha_S}$

v. Reconstruct OD_v such that $OD_v = \Theta_{SIST}\widetilde{\alpha_{OD}}$

For the exudate components:

i. Update E_v when OD_v is fixed.

ii. Calculate the pixel residuals r such that $r = I_{retina} - E_v - OD_v$

iii. Calculate non-subsampled contourlet transform Θ_{NSCT} of $E_v + r$ and obtain the coefficient vector α_E such that $\Theta_{NSCT}\ (E_v + r\ )$

iv. Hard threshold α_E with λ_v to obtain $\widetilde{\alpha_E}$

v. Reconstruct E_v such that $E_v = \Theta_{NSCT}\widetilde{\alpha_E}$

6. Update the threshold $\lambda_v = \lambda_v\, x\, \left(\frac{\lambda_0}{p\sigma}\right)^{1/(1-N_{iteration})}$ where σ is the noise standard deviation

7. if $\lambda_v > \lambda_{vmin}$, go to step 2 else finish.

8. Output: morphological components E_v and OD_v

The initial threshold λ_{vmin} was computed such as:

$$\lambda_{vmin} = \frac{1}{MN}\sum_{x-\frac{M}{2}}^{x+\frac{M}{2}}\sum_{y-\frac{N}{2}}^{y+\frac{N}{2}}P(x,y) \quad (10)$$

Where M, N are the row and columns in the bright regions and $P(x, y)$ is the pixel in the bright region.

Edge distance seeded region growing method proposed by Panda et al., (2016) was adopted to identify the true exudates out of the computed E_v. To achieve this, initial set of points called seeds were manually determined after which the neighboring pixels were visited in a particular order depending on the chosen similarity criterion.

The adopted edge distance seeded region growing is as follows:

Step 1: start

Step 2: input a set of seed pixels E_v

Step 3: choose a window size $M \times N$ from the edge image

Step 4: select a seed pixel E_v

Step 5: select a non-edge and non-seed pixel P in the window

Step 6: compute the distance PE_v between p to the nearest seed pixel E_v

Step 7: compute the distance E_vE_n between p to the nearest seed pixel E_v

Step 8: trace a line L that passes between pixels E_v and E_n

Step 9: if $PE_v < E_v\,E_n$ then the pixel is an edge pixel.

Step 10: include P in the segmented output

Step 11: repeat steps 5 to 10 until there are no more P

Step 13: stop

5.3.1 Segmenting Blood Vessels from the Diabetic Retinal Images

Segmenting blood vessels entails detecting them prior to the identification of their paths. To achieve this, preliminary vessel edge information and vessel map for the input retinal image was obtained using Dempster–Shafer (D-S) edge based detector proposed by Li & Wee, (2014). D-S uses a probability-based fusion to merge the outputs of Laplacian of Gaussian (LoG) and canny edge detection filters in determining the continuous paths of a vessel after the starting point has been determined. LoG filter was used to determine which pixels of the input retinal image is an edge pixel using equations 11, 12 and 13.

$$h(x,y) = \exp\left(-\frac{x^2+y^2}{2\sigma_N{}^2}\right) \tag{11}$$

$$\nabla^2 h(x,y) = \left(\frac{x^2+y^2-\sigma^2}{\sigma_N{}^4}\right)\exp\left(-\frac{x^2+y^2}{2\sigma_N{}^2}\right) \tag{12}$$

$$g(x,y) = \nabla^2 h(x,y) * F_{enc} \tag{13}$$

where F_{enc} remains the input enhanced foreground image, $g(x,y)$ is the output image, σ_N remains the standard deviation, $h(x,y)$ is the 2D Gaussian function and $\nabla^2 h(x,y)$ is the LoG filter.

Furthermore, in the edge detection task, after determining the edge pixels in the input image, canny filter was used to determine the horizontal, vertical, and diagonal edges. The resulting edge gradient and direction were determined using equation 14:

$$G = \sqrt{(\partial_x I(x.y))^2 + \left(\partial_y I(x.y)\right)^2} \tag{14}$$

Subsequently, the horizontal direction G_y and the vertical direction G_x were computed from gradient G using equations 15 and 16 respectively:

$$G_x = \partial_x F_{enc}(x, y) \tag{15}$$

$$G_y = \partial_y F_{enc}(x, y) \tag{16}$$

To achieve a more accurate and stable vessel edge detection, D-S based edge detector fuses the outputs $g(x, y)$ of the LoG filter and the output G of the canny edge. This is referred to as a joint $m_{1\oplus}m_2$, where $m_1 and\, m_2$ are the outputs of LoG and Canny edge filter respectively. The joint $m_{1\oplus 2}$ was obtained using equation 17 while the conflicting events caused by LoG and canny filter were removed using equation 18. The basic probability mass 'K' associated with the conflicts was calculated using equation 19.

$$m_{1\oplus}m_2(A) = \frac{\sum_{B\cap C=A} m_1(B)m_2(C)}{1-K} \tag{17}$$

$$(m_{1\oplus}m_2)_{(\ell)} = 0 \tag{18}$$

$$K = \sum_{B\cap C=\ell} m_1(B)m_2(C) \tag{19}$$

A, B and C are event set produced by the D-S fusion, LoG filter, and canny edge filter respectively.

Any edge detection algorithm could detect an edge or a non-edge vessel pixel; therefore, attempts must be made to distinguish the edge from the non-edge vessel pixel. To achieve this, the confidence level of an edge vessel pixel needs to be computed, this was represented by E while that of the non-edge vessel pixel was represented by N. Subsequently, the edge

confidence levels of the LoG filter m_1 was represented by Em_1 while that of canny filter and D-S was represented by Em_2 and E_{DS} respectively.

These confidence levels were computed using equations 20, 21 and 22 respectively.

$$Em_1 = \frac{g(x,y)}{g_{max}} \tag{20}$$

$$Em_2 = \frac{g(x,y)}{threshold} \tag{21}$$

$$E_{DS} = \frac{Em_1 Em_2}{1 - Em_1 Nm_2 - Nm_1 Em_2} \tag{22}$$

where Nm_1 is the non-edge confidence level for the LoG filter is, Nm_2 is the non-edge confidence level for canny edge filter, threshold is the max intensity gradient value. The non-edge confidence level for the D-S filter NE_{DS} was calculated using equation 23:

$$NE_{DS} = 1 - E_{DS} \tag{23}$$

5.4 Extracting Features from Retinal Images

A total of sixteen (16) features in three categories were extracted from the retinal images. Lesion based and morphological features were extracted from DR retinal images using connected component analysis and statistical techniques respectively while image based structural features such as luminance, contrast and structure were computed from healthy retinal images.

5.4.1 Extracting Features from Healthy Retinal Images

Since healthy retinal images are clean and do not have pathological symptoms, structural features that define the relationship between its components were computed. These are luminance, contrast and structure; they are computed using mathematical formulas highlighted in equations 24, 25 and 26 respectively.

Luminance Feature $(f_1) = \frac{2\mu_N + C}{{\mu_N}^2}$ (24)

Contrast Feature (f_2) = $\frac{2\sigma_N + C}{\sigma_N{}^2}$ (25)

Structure Feature (f_3) = $\frac{2\sigma_N + C}{\sigma_N + C}$ (26)

Where μ_N remains the mean intensity of the image, σ_N remains the standard deviation of the intensity and C is a constant used to avoid instability, it was calculated using equation 27.

$C = (KL)^2$ (27)

Where L is the range of pixel values i.e. 255 (256-1 for 8 bit gray scale image) and k is a value $\ll 1$, 0.01 was preferred after considering different values.

Finally, extracted features from the healthy images were saved in a features database for matching purpose.

5.4.2 Extracting Features from Diabetic Retinopathy Images

Morphological and lesion based features were extracted from diabetic retinopathy images.

a) Extracting Morphological Features from the Segmented Blood Vessels

Six morphological features as enumerated below were computed and extracted from the segmented blood vessels of diabetic retinopathy images:

1. Vessel diameters(f_4): This is the mean width of blood vessels in the input retina image. It is defined as the shortest line segment (Euclidean distance) between two edges A and B of a blood vessel wall. The Euclidean distance was computed using equation 28:

   $E_D = \sqrt{|X_A - X_B|^2 + |Y_A - Y_B|^2}$ (28)

   $if\ E_D \geq 11$, it is a main vessel, if $4 \leq E_D \leq 7$ it is a secondary vessel while if $2 \leq E_D < 3$ it is a vascular vessel.
2. Lines(f_5): these are straight paths between two pixels.
3. Branch points(f_6): these are points where a pixel originates from.
4. Ridges end points (f_7): these are where the curved lines of a pixel terminate.

5. Bifurcation points (f_8): these are points where two ridges come together or where a pixel divides into two branches.
6. Bifurcations and ridge endings (minutiae)(f_9): these are points where blood vessels divide into two branches and where they terminate.

Connected component analysis proposed by Sasidharan, (2014) which measures the degree of connectivity of the image pixels called connectivity number c_n was used to determine and measure morphological features $f_5 - f_9$. If $c_n = 1$ then it is a vessel end point, if $c_n = 2$, it is a line, if $c_n = 3$, it is a bifurcation point, if $c_n = 4$, it is a cross over point. If $c_n = 2$ & 1 it is a bifurcation end.

b) Extracting Lesion based Features from the Segmented Exudate Regions

Finally, seven lesion based features were extracted from the exudates of the diabetic retinal images using statistical techniques. The features are discussed below:

1. Extent(f_{10}): this is the ratio of pixels in the exudate regions to the pixels in the whole image. Extent should have a low value for true exudates detected compared to the false vessel segment.
2. Major axis length(f_{11}): this is the length of major axis of the exudate regions. The value of major axis length should be high for exudate regions compared to non-exudate regions.
3. Filled area (f_{12}): this is the number of pixels in the filled image. This should yield a high value for false exudate regions and have more number of pixels in the exudate region than non-exudate regions
4. MeanIntensity (f_{13}): This calculates the mean of all intensity values in the whole image. Non-exudate regions should have a uniform high mean intensity value while exudate regions should have an uneven low mean intensity value.

5. MaxIntensity (f_{14}): This measures the highest intensities in the whole image. The value should be low for the segmented exudate region while non-exudate regions should have a high value.
6. Energy(f_{15}): this is a measure of the sum of intensity squares of all pixel values within the exudate regions.
7. Compactness(f_{16}): this is a measure of the shape of the exudate regions. It was computed using equation 29

$$f_{16} = \frac{p^2}{4\pi A} \tag{29}$$

where the segmented region is symbolized by A and p is the perimeter of the exudate region. The block diagram of the develop system is shown in Figure 13.

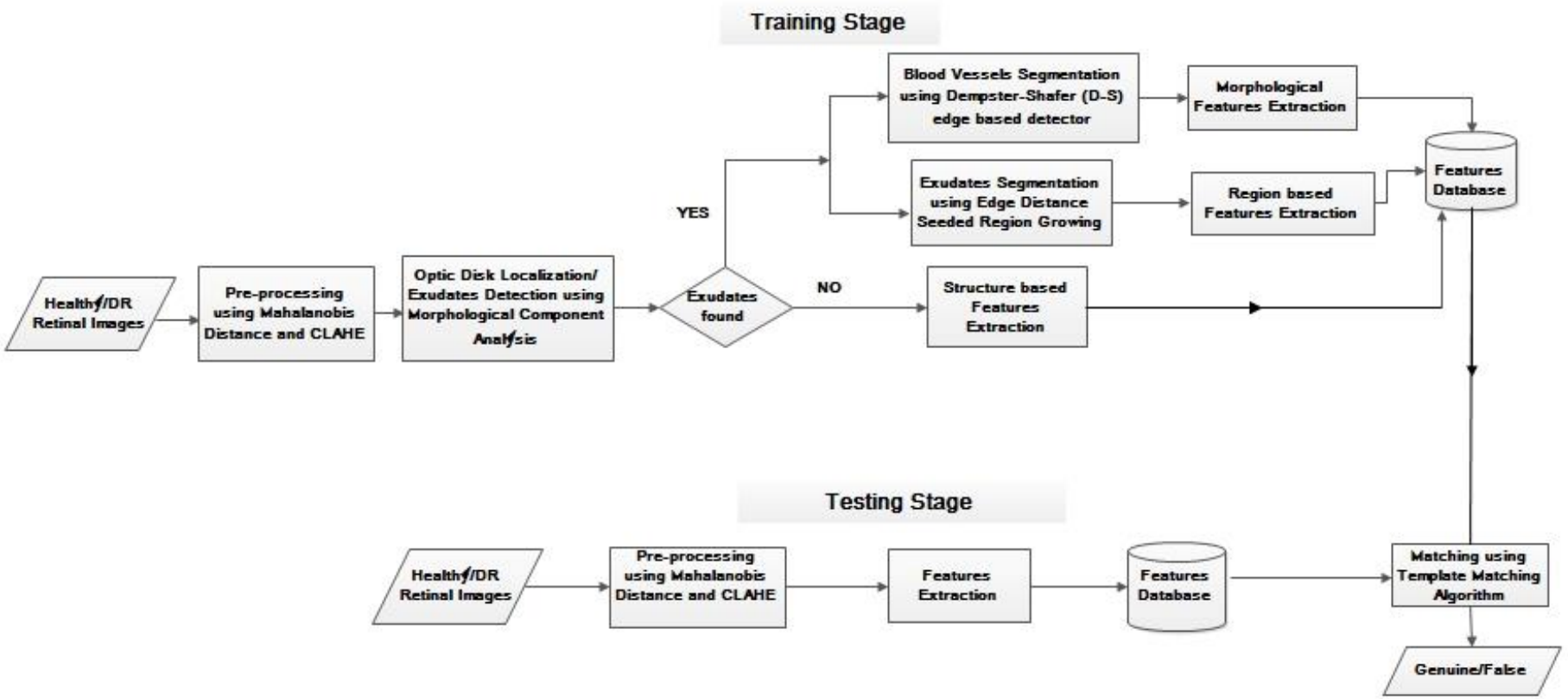

Figure 13: Block Diagram of the Develop System

5.5 Programming Tool Adopted

The implementation of the algorithms discussed in this research was carried out using Matrix Laboratory (MATLAB) R2015a programing environment installed on a 64bit intel dual core HP laptop.

6. RESULTS AND DISCUSSIONS

This section discusses in details some of the results obtained from the proposed research.

6.1 Training the Developed System

After implementing the algorithms proposed at each stage of the research, the developed system was trained with selected healthy as well as DR retinal images. A total of thirty (30) healthy and DR retinal images were randomly selected from DRIVE, STARE, DIARETDB1, DRiDB and CPRD databases for the training purpose while sixty (60) images were used for testing. The time taken to train each retina image is shown in Figure 14 while the numeric features extracted from the trained images were shown in Figure 15. A 30 x 16 feature matrix was produced to connote thirty (30) images used for the training and sixteen (16) features extracted.

6.2 The Preprocessed Retina Images

All the retina images used were preprocessed so as to make them suitable for features extraction. The preprocessing entails extracting the green component (as shown in Figure 16) from the input images since it has the best contrast and less noise. Afterwards, the green component of the image was converted to a grayscale image by eliminating its hue and saturation component while the luminance was retained; the output green component is shown in Figure 17. Preprocessing also involves smoothening and removing noise from the input retinal image; these were achieved using median filtering (as shown in Figure 18). Afterwards,

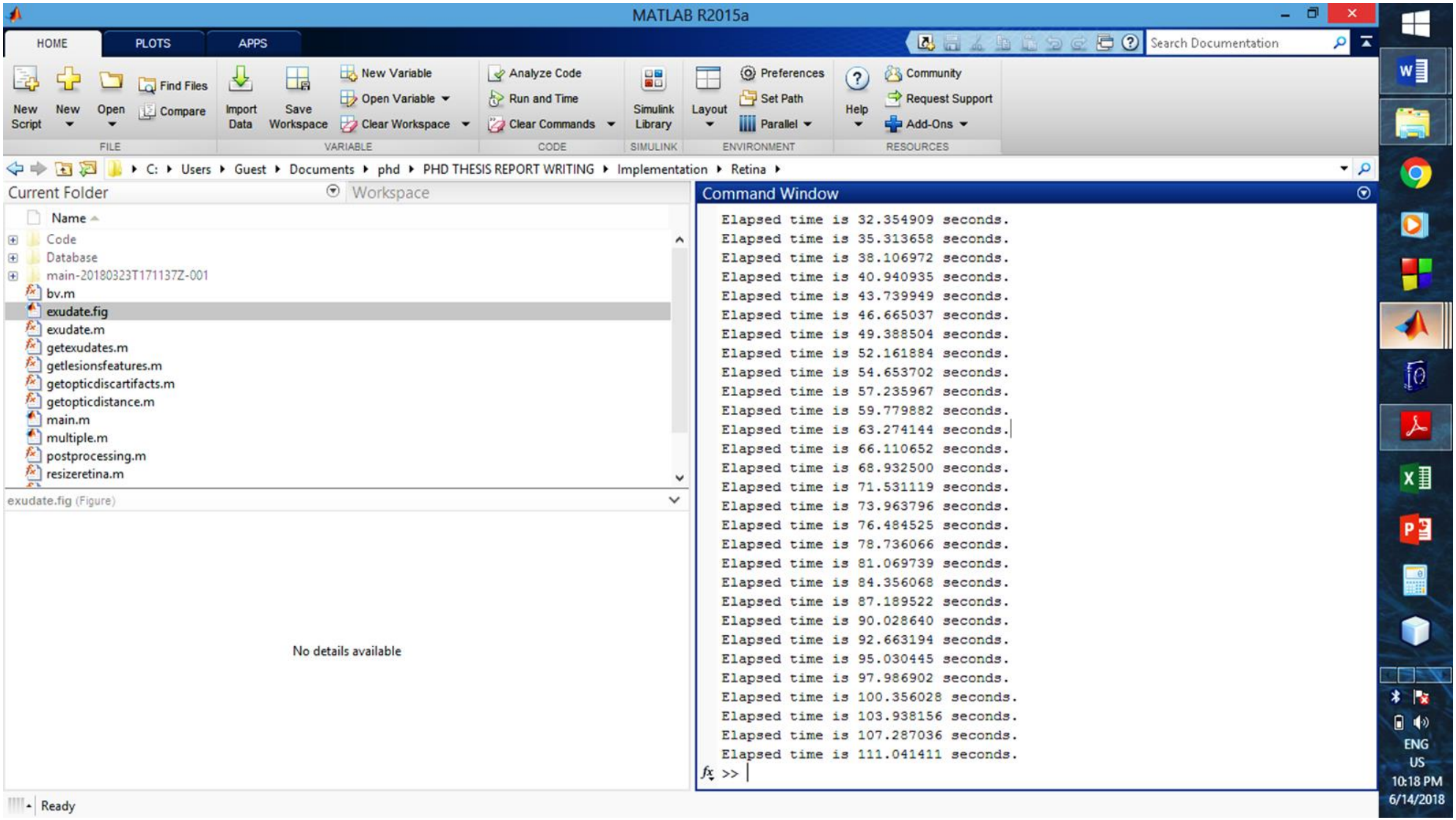

Figure 14: Time Taken to Train each Retina Image

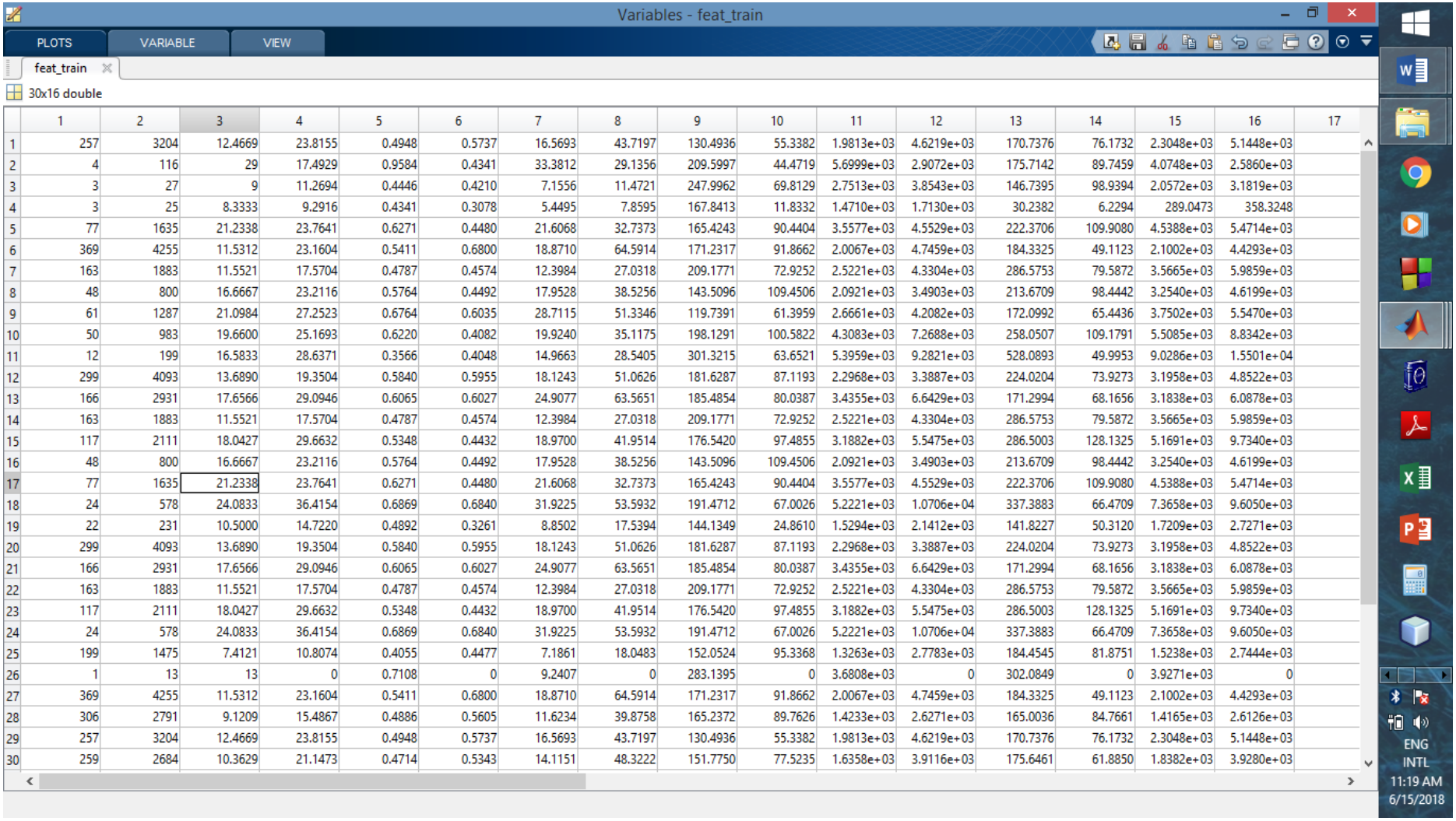

	1	2	3	4	5	6	7	8	9	10	11	12	13	14	15	16	17
1	257	3204	12.4669	23.8155	0.4948	0.5737	16.5693	43.7197	130.4936	55.3382	1.9813e+03	4.6219e+03	170.7376	76.1732	2.3048e+03	5.1448e+03	
2	4	116	29	17.4929	0.9584	0.4341	33.3812	29.1356	209.5997	44.4719	5.6999e+03	2.9072e+03	175.7142	89.7459	4.0748e+03	2.5860e+03	
3	3	27	9	11.2694	0.4446	0.4210	7.1556	11.4721	247.9962	69.8129	2.7513e+03	3.8543e+03	146.7395	98.9394	2.0572e+03	3.1819e+03	
4	3	25	8.3333	9.2916	0.4341	0.3078	5.4495	7.8595	167.8413	11.8332	1.4710e+03	1.7130e+03	30.2382	6.2294	289.0473	358.3248	
5	77	1635	21.2338	23.7641	0.6271	0.4480	21.6068	32.7373	165.4243	90.4404	3.5577e+03	4.5529e+03	222.3706	109.9080	4.5388e+03	5.4714e+03	
6	369	4255	11.5312	23.1604	0.5411	0.6800	18.8710	64.5914	171.2317	91.8662	2.0067e+03	4.7459e+03	184.3325	49.1123	2.1002e+03	4.4293e+03	
7	163	1883	11.5521	17.5704	0.4787	0.4574	12.3984	27.0318	209.1771	72.9252	2.5221e+03	4.3304e+03	286.5753	79.5872	3.5665e+03	5.9859e+03	
8	48	800	16.6667	23.2116	0.5764	0.4492	17.9528	38.5256	143.5096	109.4506	2.0921e+03	3.4903e+03	213.6709	98.4442	3.2540e+03	4.6199e+03	
9	61	1287	21.0984	27.2523	0.6764	0.6035	28.7115	51.3346	119.7391	61.3959	2.6661e+03	4.2082e+03	172.0992	65.4436	3.7502e+03	5.5470e+03	
10	50	983	19.6600	25.1693	0.6220	0.4082	19.9240	35.1175	198.1291	100.5822	4.3083e+03	7.2688e+03	258.0507	109.1791	5.5085e+03	8.8342e+03	
11	12	199	16.5833	28.6371	0.3566	0.4048	14.9663	28.5405	301.3215	63.6521	5.3959e+03	9.2821e+03	528.0893	49.9953	9.0286e+03	1.5501e+04	
12	299	4093	13.6890	19.3504	0.5840	0.5955	18.1243	51.0626	181.6287	87.1193	2.2968e+03	3.3887e+03	224.0204	73.9273	3.1958e+03	4.8522e+03	
13	166	2931	17.6566	29.0946	0.6065	0.6027	24.9077	63.5651	185.4854	80.0387	3.4355e+03	6.6429e+03	171.2994	68.1656	3.1838e+03	6.0878e+03	
14	163	1883	11.5521	17.5704	0.4787	0.4574	12.3984	27.0318	209.1771	72.9252	2.5221e+03	4.3304e+03	286.5753	79.5872	3.5665e+03	5.9859e+03	
15	117	2111	18.0427	29.6632	0.5348	0.4432	18.9700	41.9514	176.5420	97.4855	3.1882e+03	5.5475e+03	286.5003	128.1325	5.1691e+03	9.7340e+03	
16	48	800	16.6667	23.2116	0.5764	0.4492	17.9528	38.5256	143.5096	109.4506	2.0921e+03	3.4903e+03	213.6709	98.4442	3.2540e+03	4.6199e+03	
17	77	1635	21.2338	23.7641	0.6271	0.4480	21.6068	32.7373	165.4243	90.4404	3.5577e+03	4.5529e+03	222.3706	109.9080	4.5388e+03	5.4714e+03	
18	24	578	24.0833	36.4154	0.6869	0.6840	31.9225	53.5932	191.4712	67.0026	5.2221e+03	1.0706e+04	337.3883	66.4709	7.3658e+03	9.6050e+03	
19	22	231	10.5000	14.7220	0.4892	0.3261	8.8502	17.5394	144.1349	24.8610	1.5294e+03	2.1412e+03	141.8227	50.3120	1.7209e+03	2.7271e+03	
20	299	4093	13.6890	19.3504	0.5840	0.5955	18.1243	51.0626	181.6287	87.1193	2.2968e+03	3.3887e+03	224.0204	73.9273	3.1958e+03	4.8522e+03	
21	166	2931	17.6566	29.0946	0.6065	0.6027	24.9077	63.5651	185.4854	80.0387	3.4355e+03	6.6429e+03	171.2994	68.1656	3.1838e+03	6.0878e+03	
22	163	1883	11.5521	17.5704	0.4787	0.4574	12.3984	27.0318	209.1771	72.9252	2.5221e+03	4.3304e+03	286.5753	79.5872	3.5665e+03	5.9859e+03	
23	117	2111	18.0427	29.6632	0.5348	0.4432	18.9700	41.9514	176.5420	97.4855	3.1882e+03	5.5475e+03	286.5003	128.1325	5.1691e+03	9.7340e+03	
24	24	578	24.0833	36.4154	0.6869	0.6840	31.9225	53.5932	191.4712	67.0026	5.2221e+03	1.0706e+04	337.3883	66.4709	7.3658e+03	9.6050e+03	
25	199	1475	7.4121	10.8074	0.4055	0.4477	7.1861	18.0483	152.0524	95.3368	1.3263e+03	2.7783e+03	184.4545	81.8751	1.5238e+03	2.7444e+03	
26	1	13	13	0	0.7108	0	9.2407	0	283.1395	0	3.6808e+03	0	302.0849	0	3.9271e+03	0	
27	369	4255	11.5312	23.1604	0.5411	0.6800	18.8710	64.5914	171.2317	91.8662	2.0067e+03	4.7459e+03	184.3325	49.1123	2.1002e+03	4.4293e+03	
28	306	2791	9.1209	15.4867	0.4886	0.5605	11.6234	39.8758	165.2372	89.7626	1.4233e+03	2.6271e+03	165.0036	84.7661	1.4165e+03	2.6126e+03	
29	257	3204	12.4669	23.8155	0.4948	0.5737	16.5693	43.7197	130.4936	55.3382	1.9813e+03	4.6219e+03	170.7376	76.1732	2.3048e+03	5.1448e+03	
30	259	2684	10.3629	21.1473	0.4714	0.5343	14.1151	48.3222	151.7750	77.5235	1.6358e+03	3.9116e+03	175.6461	61.8850	1.8382e+03	3.9280e+03	

Figure 15: Features Extracted from the Trained Retina Images

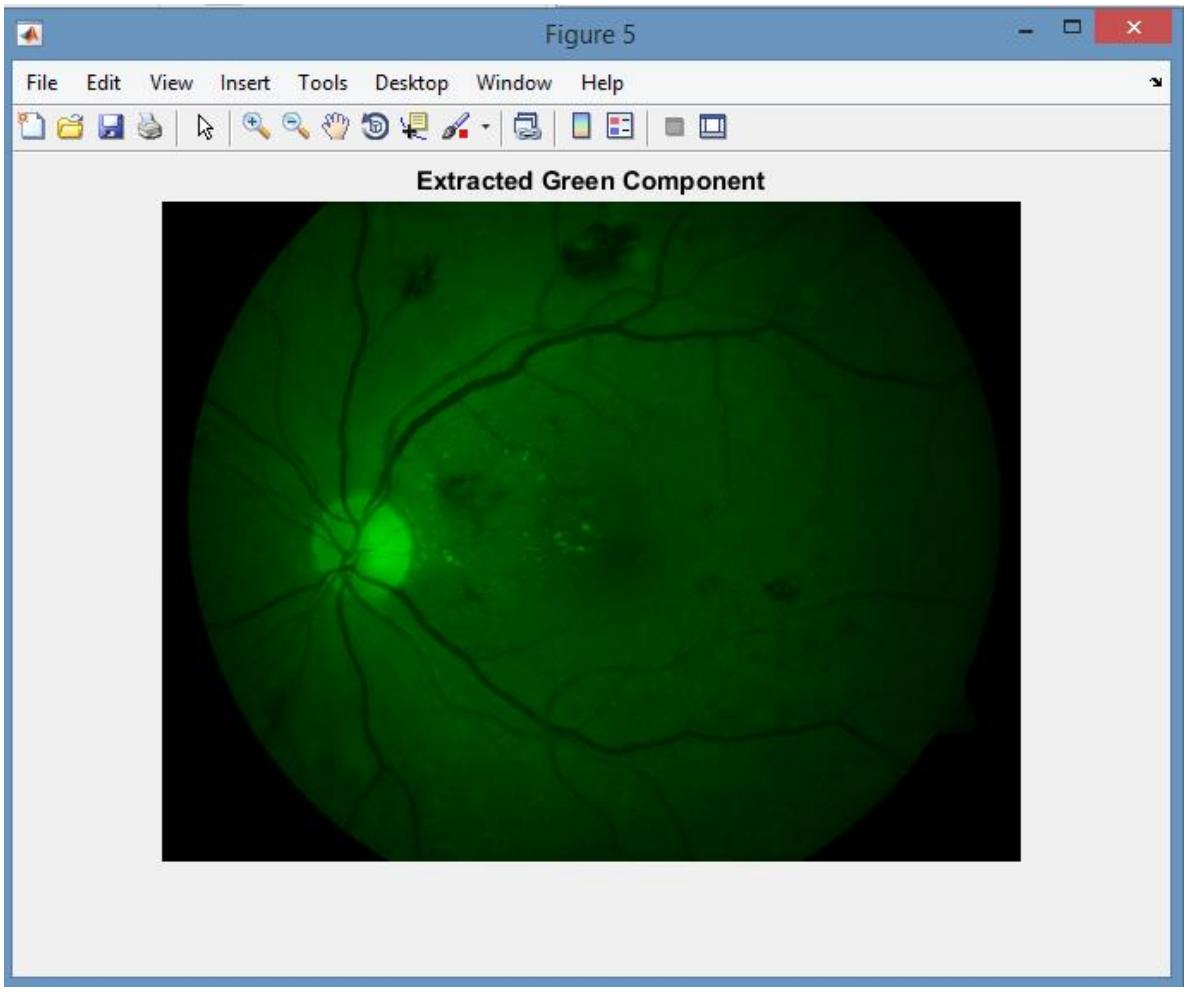

Figure 16: Green Component Extracted from Coloured Retina Images

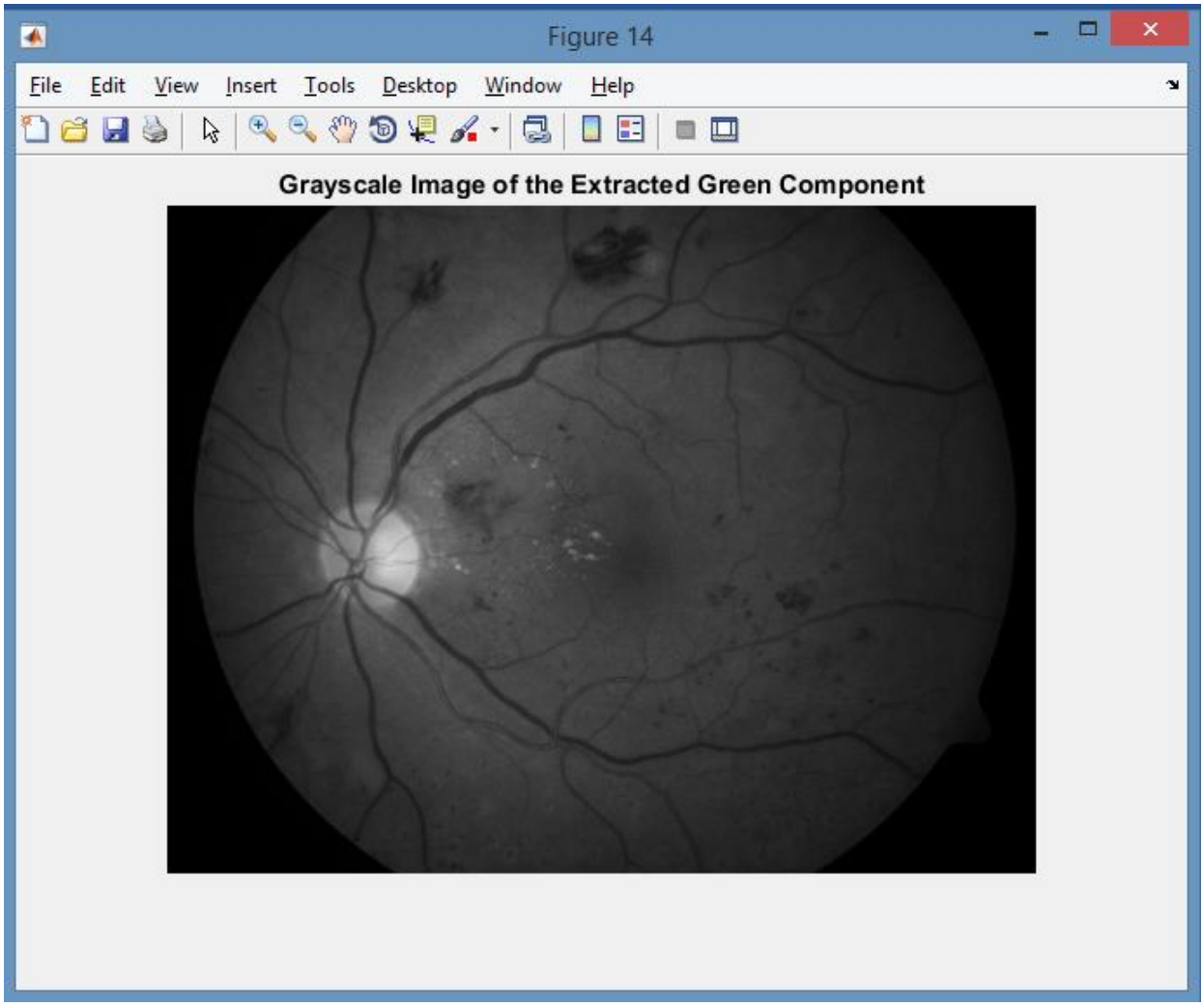

Figure 17: Grayscale Image of the Extracted Green Component

Figure 18: Grayscale Image after Median Filtering

the contrast of the retinal image was enhanced using Mahalanobis distance with CLAHE (as shown in Figure 19).

6.3 Optic Disk Localization and Extraction

After preprocessing the images, the optic disk (especially in the DR retinal images) needs to be located and removed. This is because optic disc and exudates are the only bright regions in the retinal image. Optic disc in the healthy retina image need not be removed since healthy retina image is believed to be devoid of exudates. The location and size of the optic disc was finally calculated by varying the threshold value T initially calculated using equation 10. When threshold value 0.80 was used for image 8, an imperfect optic disc was located (as shown in Figure 20). However, a perfect optic disc was located and removed at threshold 0.50; these are shown in Figures 21 and 22.

6.4 Features Extracted from Healthy Retinal Images

Since healthy retina images have clean components, structural features such as luminance, contrast and structure were extracted as shown in Figure 23.

6.5 Features Extracted from DR Retinal Images

To ensure an all-out identification of DR retinal images; six morphological and seven lesion based features were extracted from the segmented blood vessels as shown in Figure 24 and exudates as shown in Figure 25 respectively.

Afterwards, morphological features such as mean vessel diameters (as shown in Figure 26), vessel lines (as shown in Figure 27), branch points (as shown in Figure 28), ridges end points (as shown in Figure 29), bifurcation points (as shown in Figure 30), bifurcations and ridge endings (as shown in Figure 31) were all extracted from the segmented blood vessels. Furthermore, exudates were segmented from DR retinal images (as shown in Figure 32) using edge seeded region growing method. Seven lesion based features were then extracted from the exudates. They are shown in Figure 33.

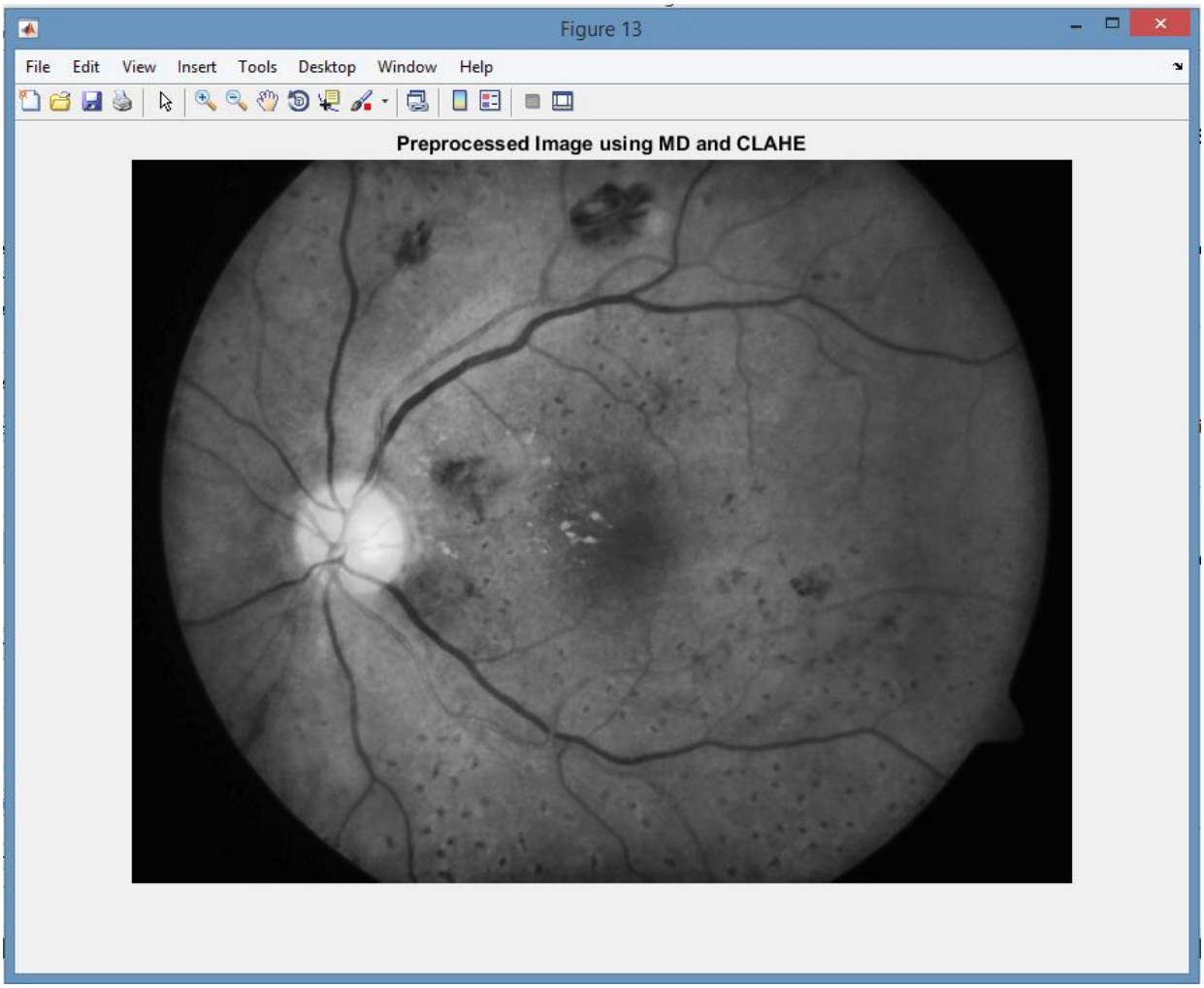

Figure 19: Grayscale Image after Applying Mahalanobis Distance and CLAHE

Figure 20: Optic Disc located and Extracted in the Input DR Retinal Image at Threshold 0.80

Figure 21: Optic Disc Located and Extracted in the Input DR Retinal Image at Threshold 0.50

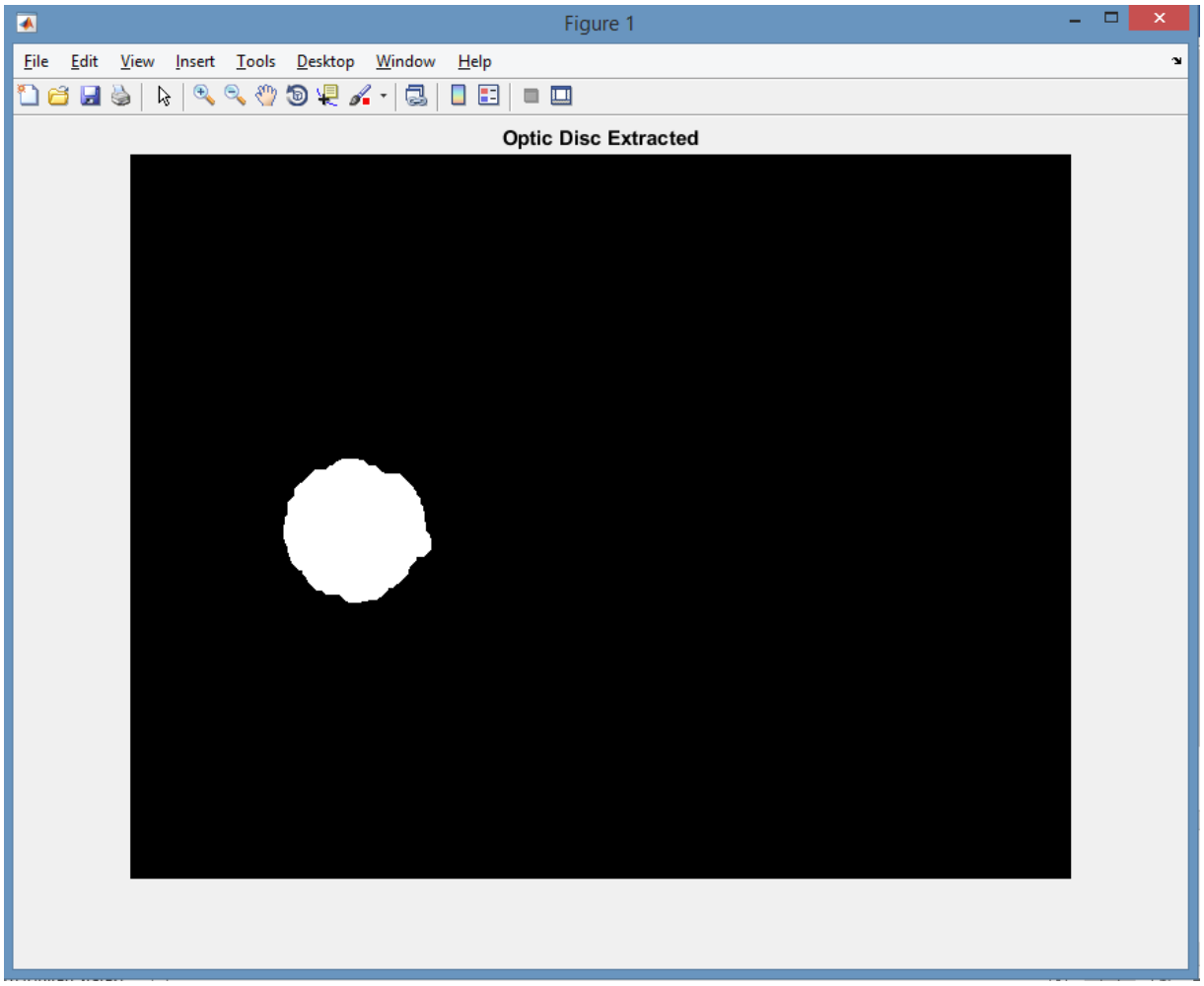

Figure 22: Extracted Optic Disc in the Input DR Retinal Image at Threshold 0.50

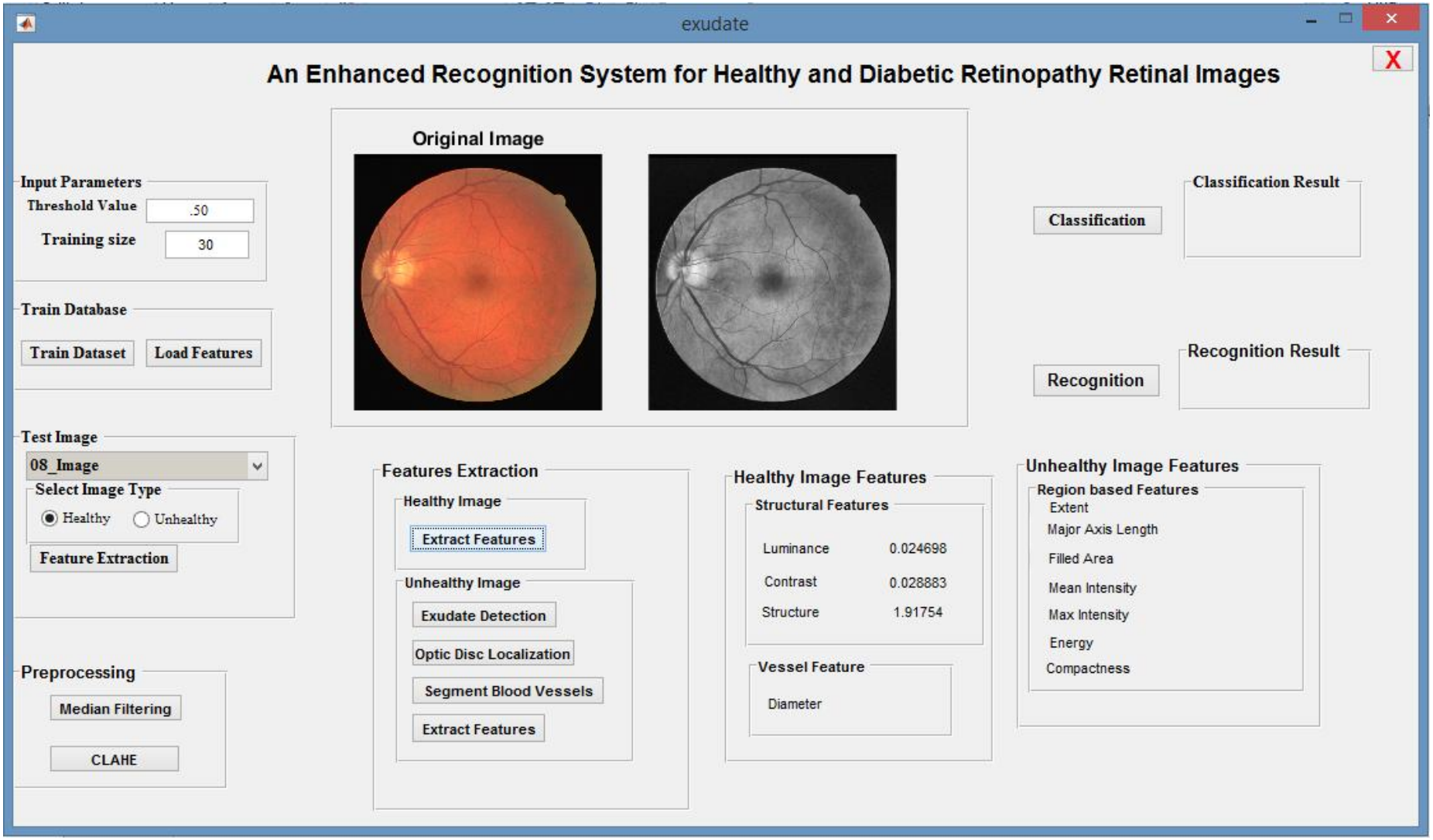

Figure 23: Structural Features Computed from the Healthy Retina Image

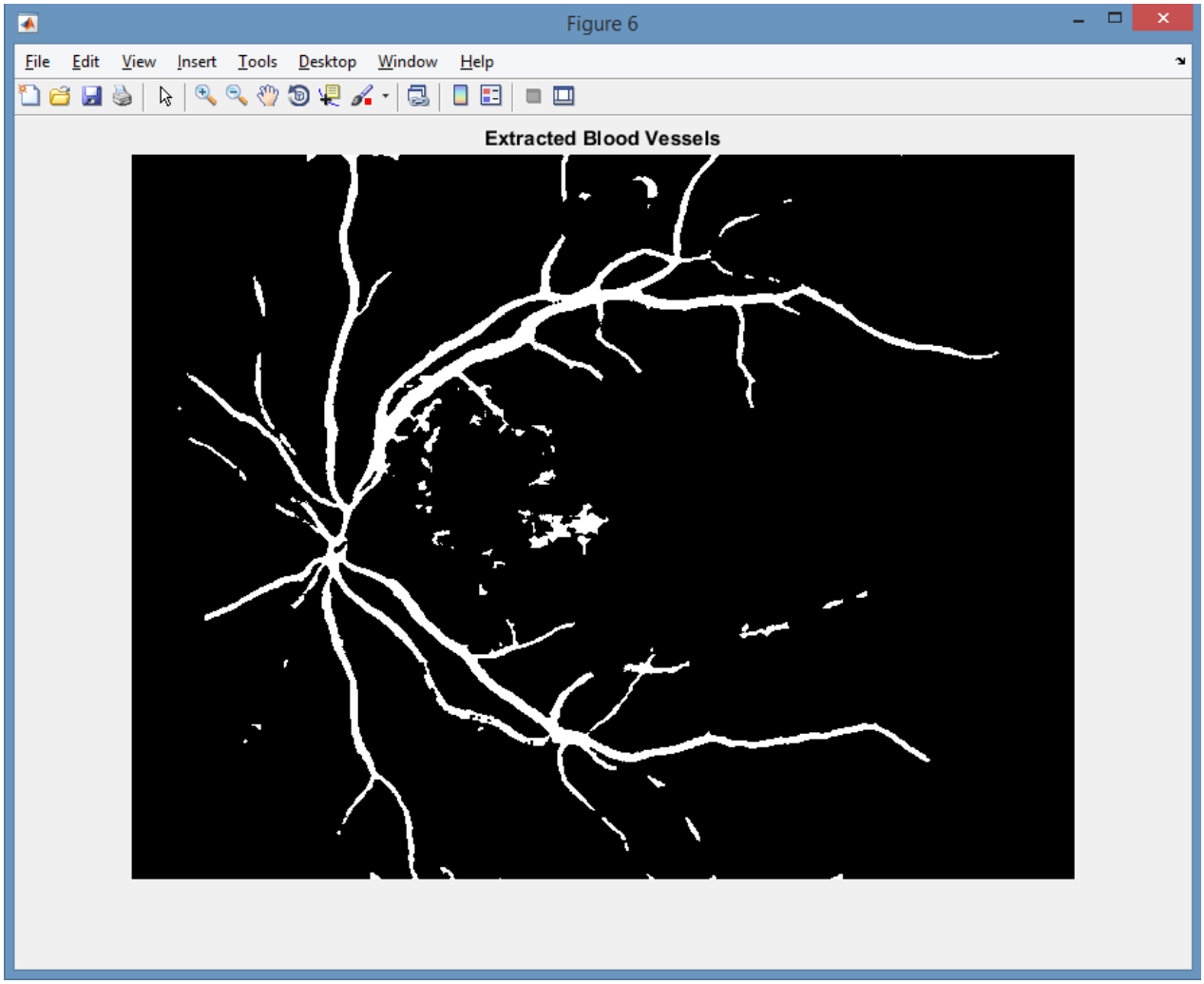

Figure 24: Extracted Blood Vessels from DR Retina Image

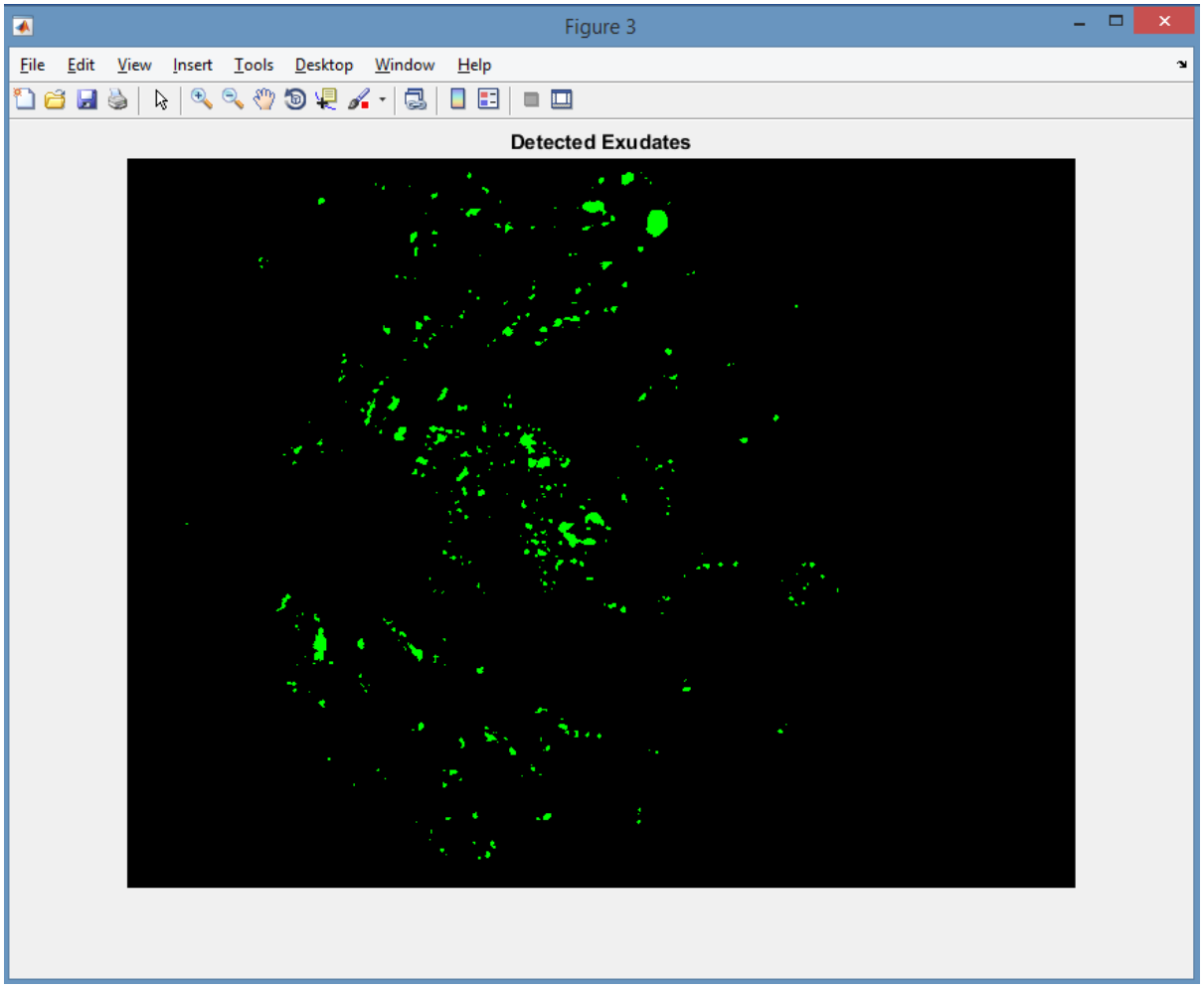

Figure 25: Detected and Extracted Exudates from the DR Retina Image

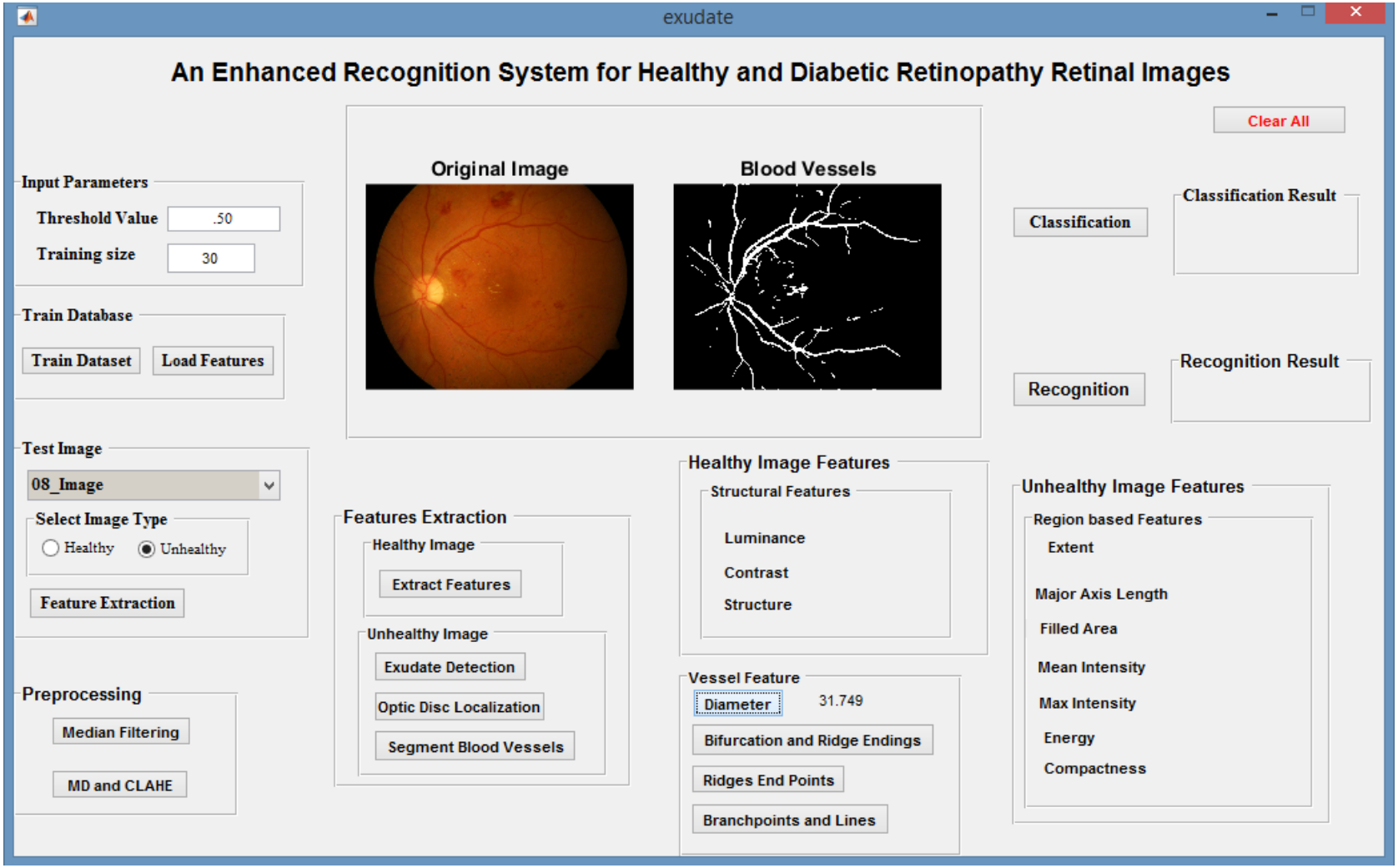

Figure 26: Computed Mean Diameter of the Extracted Blood Vessels

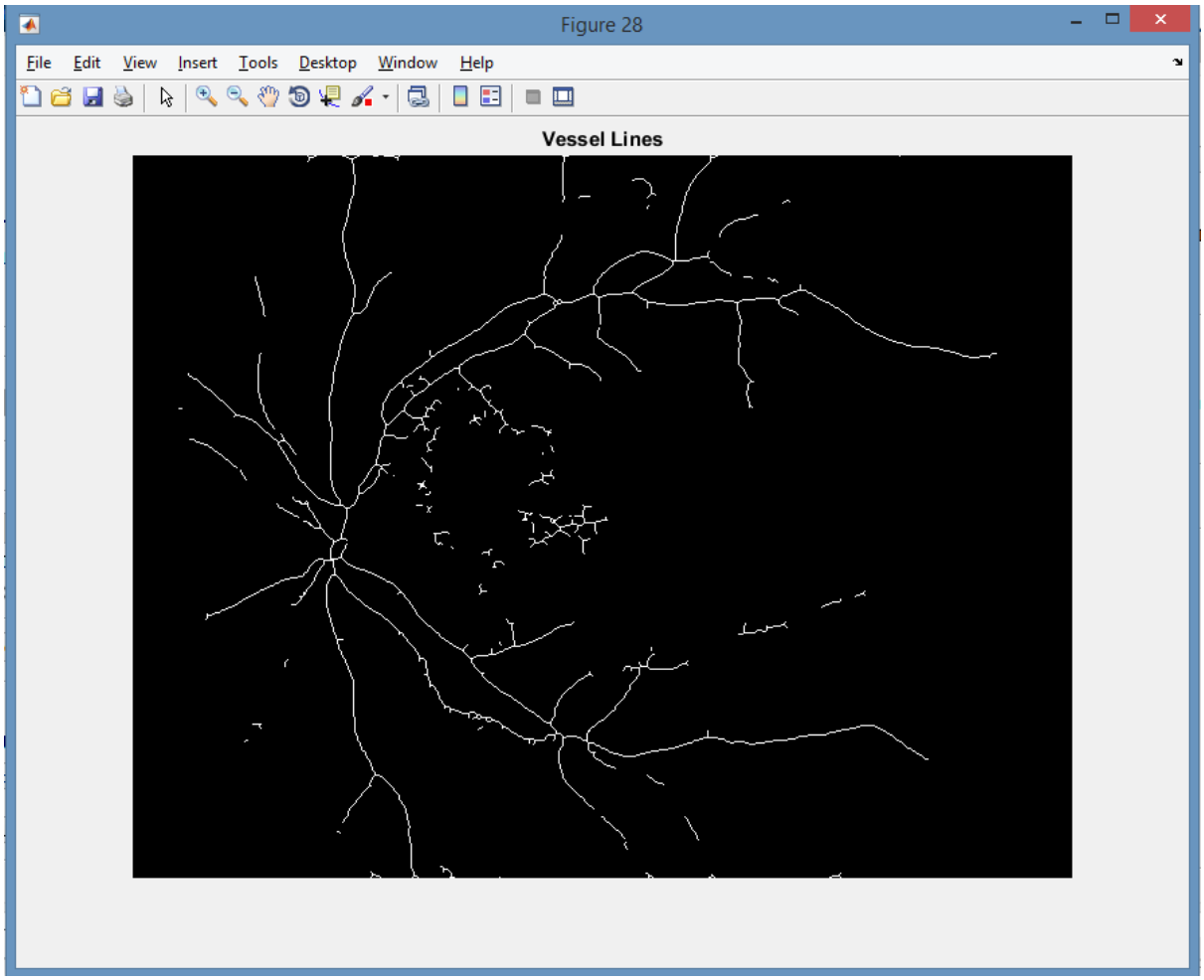

Figure 27: Blood Vessel Lines Extracted from the Blood Vessel

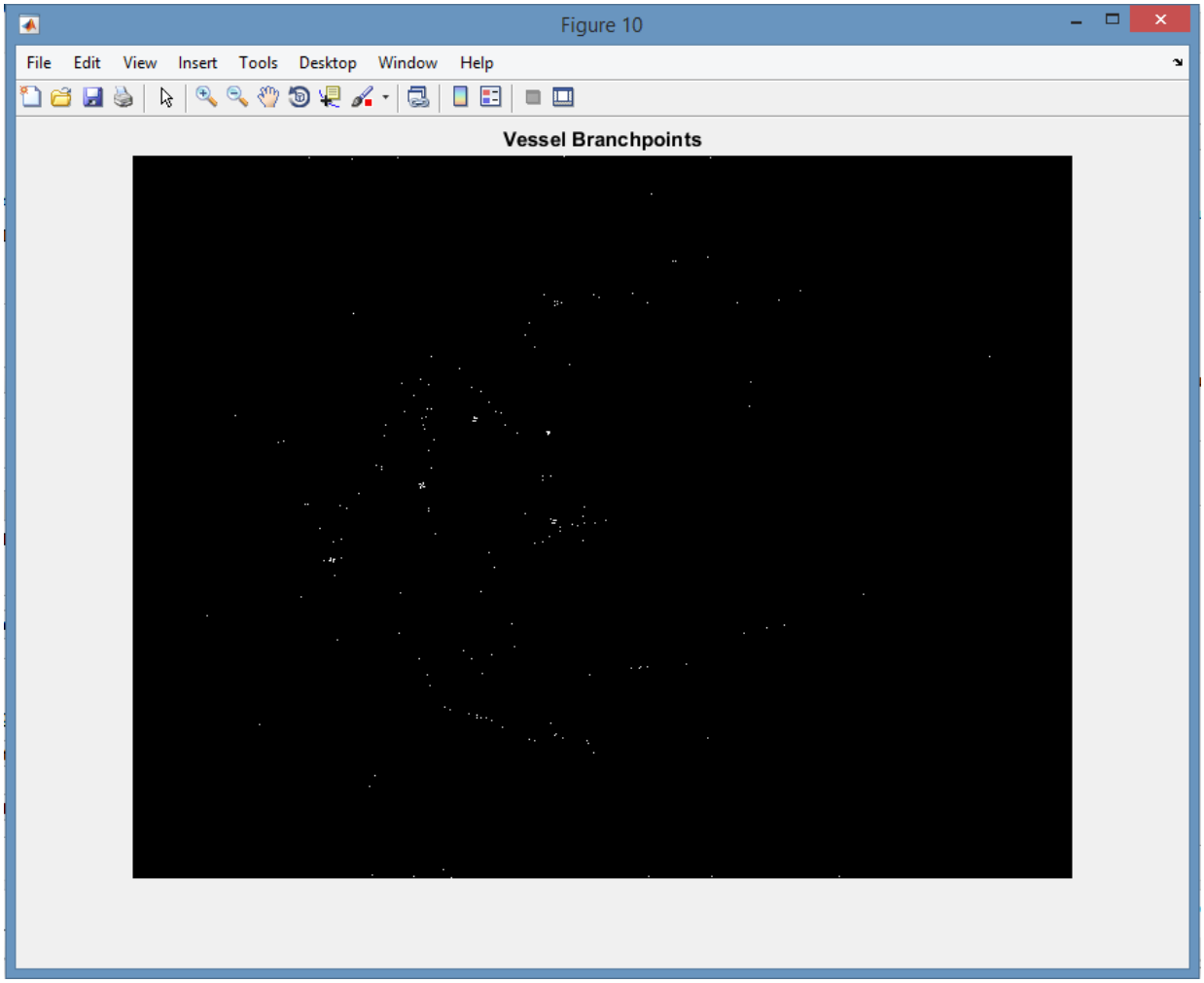

Figure 28: Vessel Branch Points Extracted from the Blood Vessel

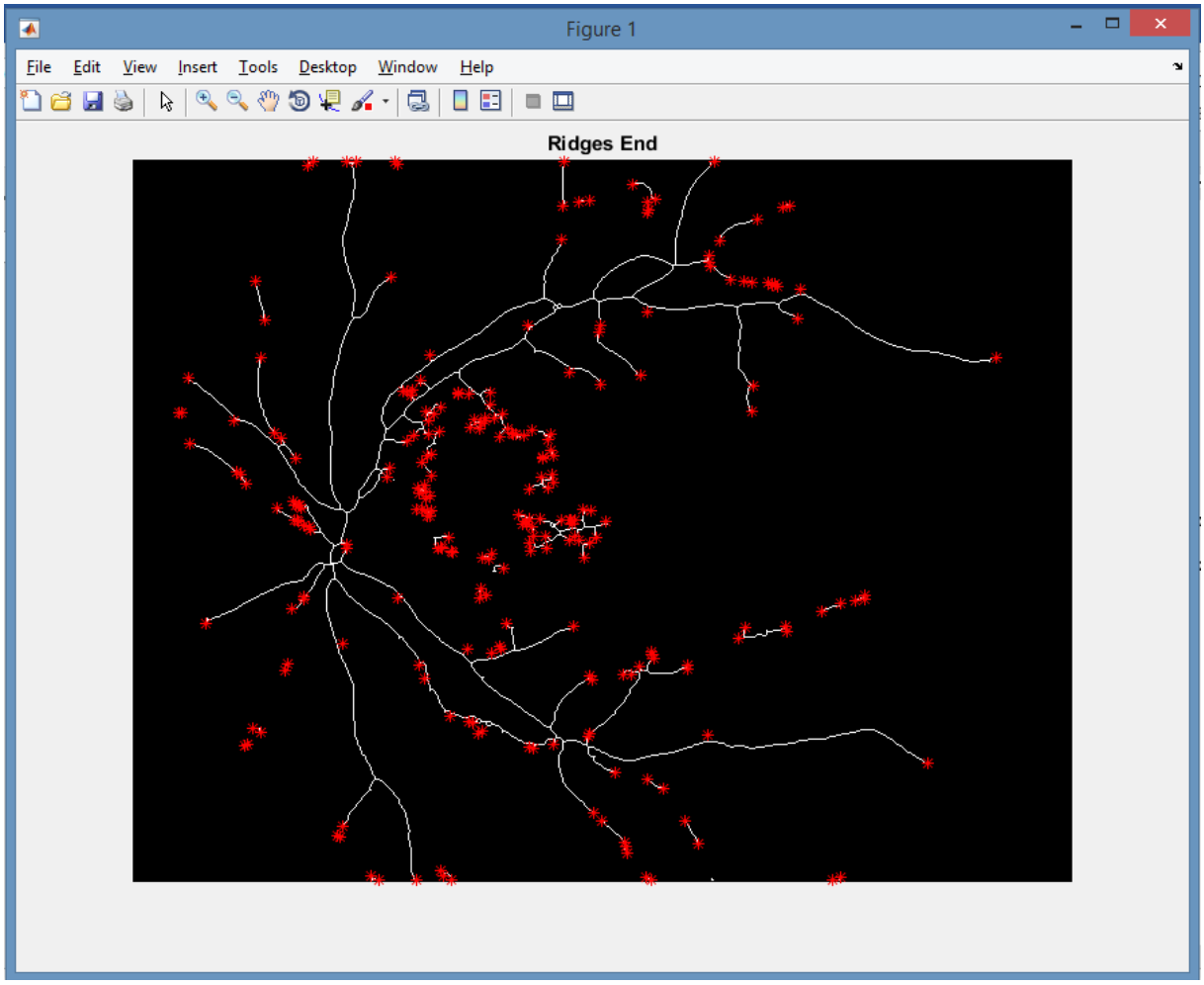

Figure 29: Ridges Endpoints Extracted from the Blood Vessel

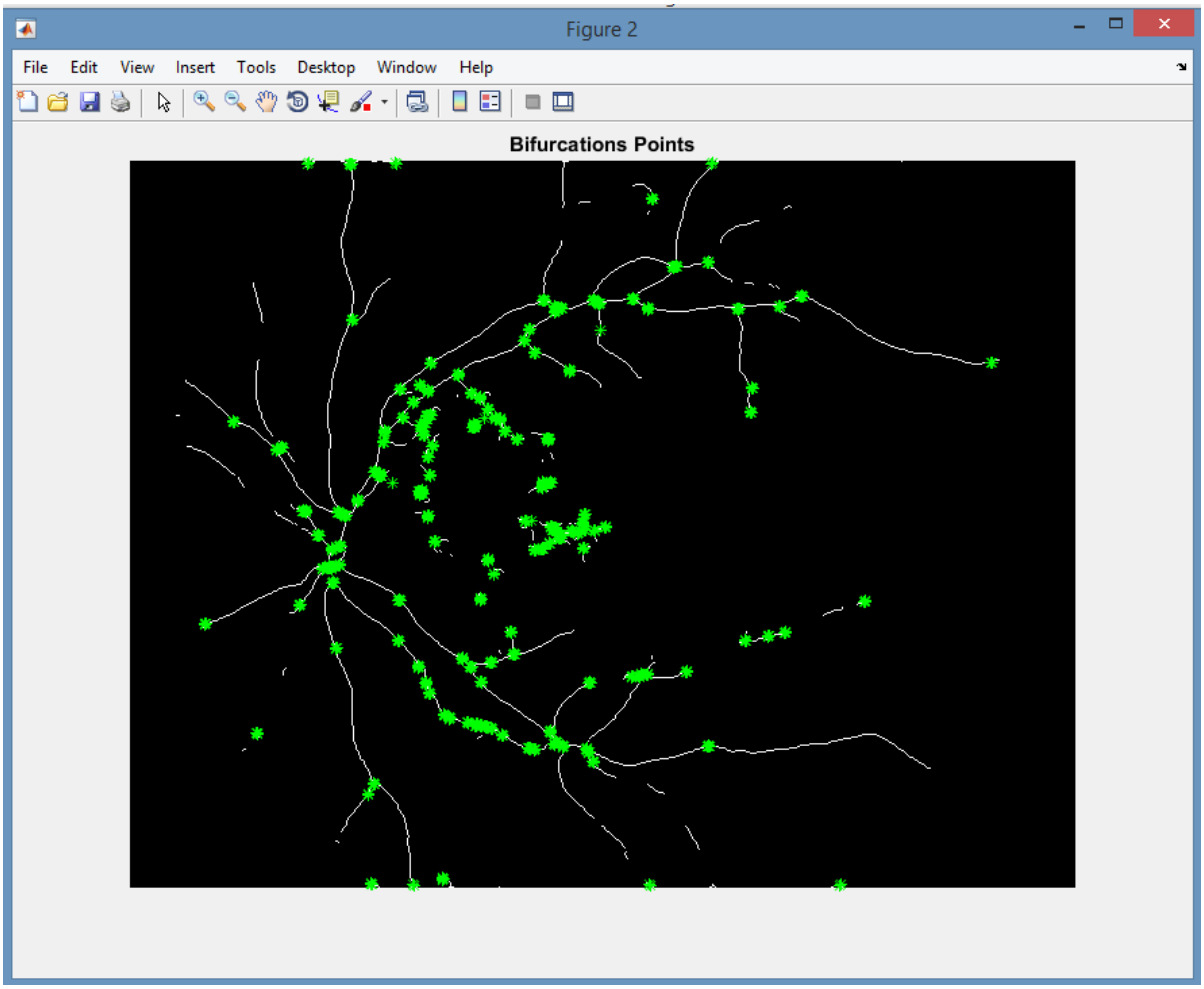

Figure 30: Bifurcation Points Extracted from the Blood Vessel

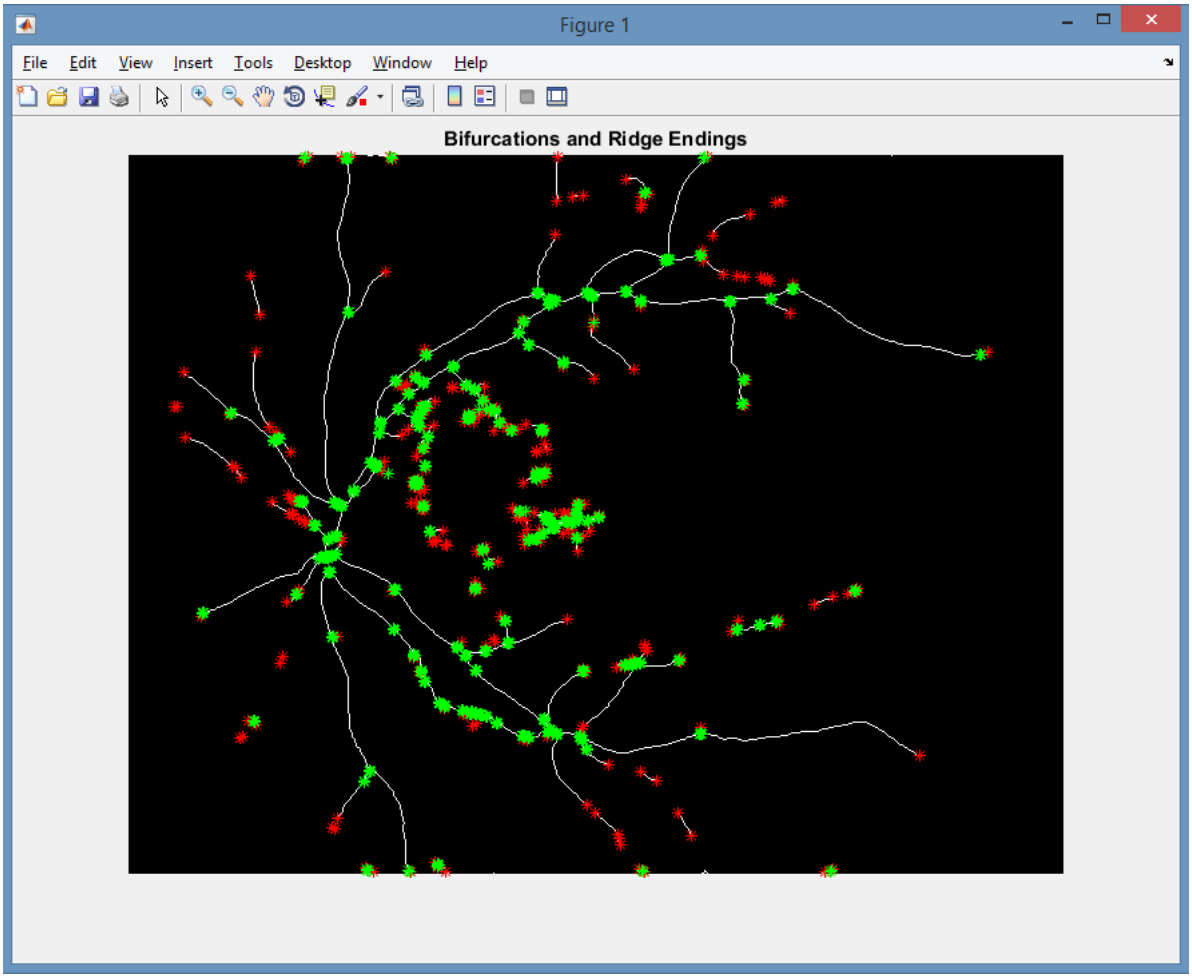

Figure 31: Bifurcation and Ridge Endings Extracted from the Blood Vessel

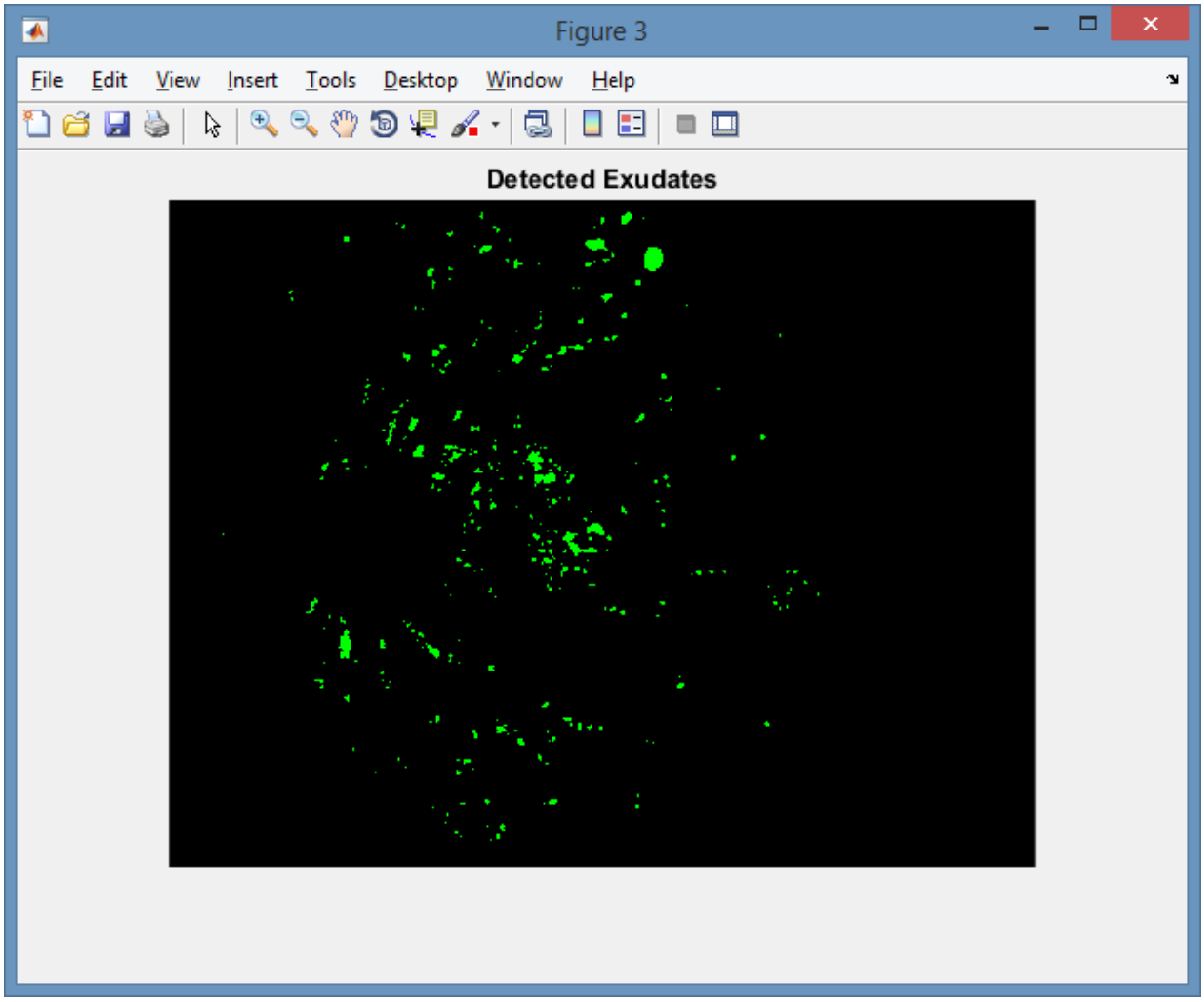

Figure 32: Exudates Detected and Extracted from DR Retinal Images

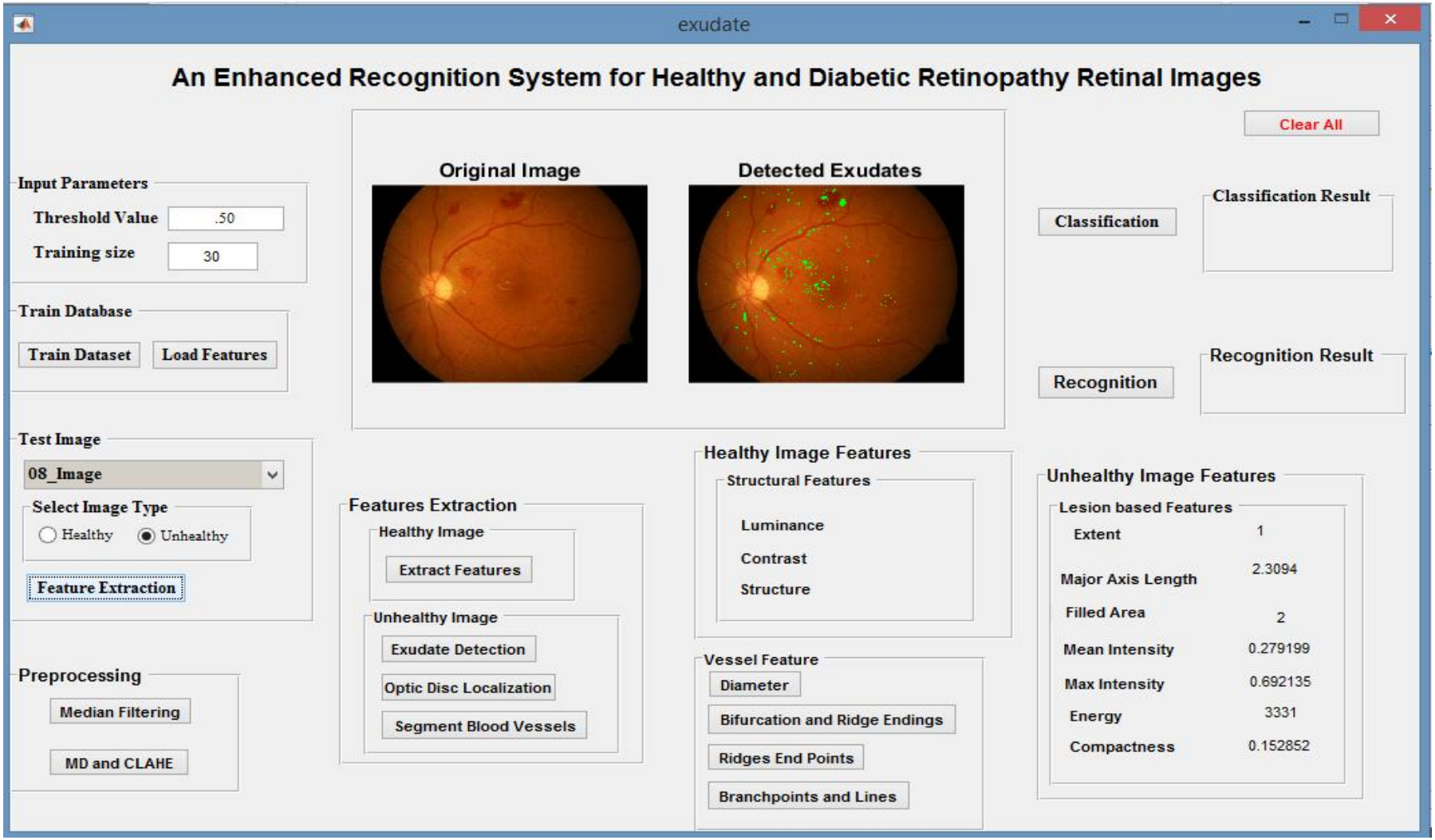

Figure 33: Lesion based Features Extracted from DR Retinal Image

To further examine the effect of DR on retinal images, blood vessels were extracted from healthy retinal images (as shown in Figure 34) and compared with those extracted from DR retina images as shown in Figure 35. This comparison revealed the extent of disappearance of blood vessels which further affirmed the extent of damages that DR could inflict on a retina. A comparison of the blood vessels diameter in healthy ($16.2369m^2$) and unhealthy retinal images (31.749) also confirmed that DR leads to a massive increase in the diameter and explosion of blood vessels. The general overview of the whole feature extraction stage is presented in Figure 36.

Having meticulously extracted features from both healthy and DR retinal images, it is conjectured that the proposed recognition system based on the extracted features should be able to identify healthy as well as DR individual.

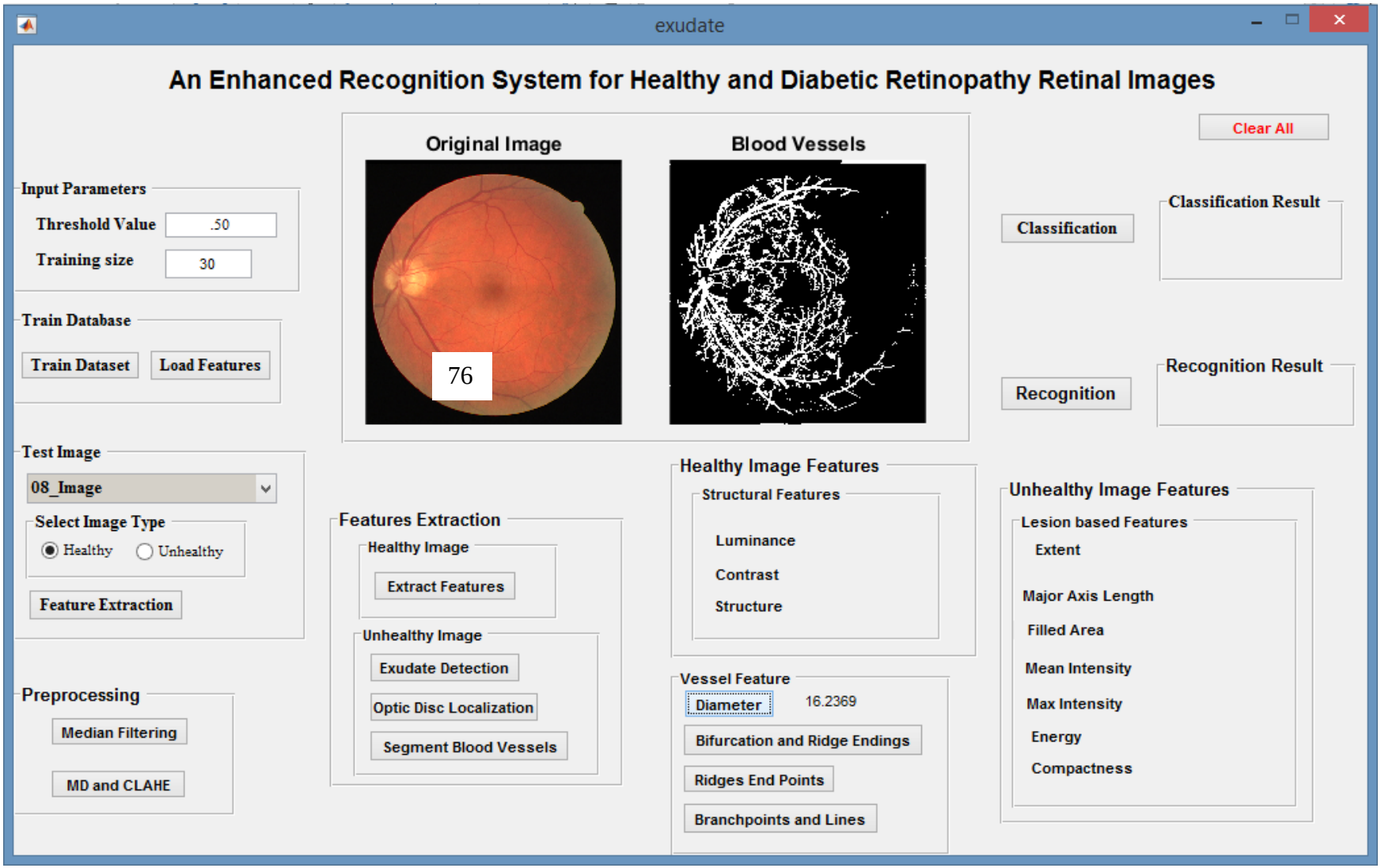

Figure 34: Blood Vessels Segmented from Healthy Retinal Image

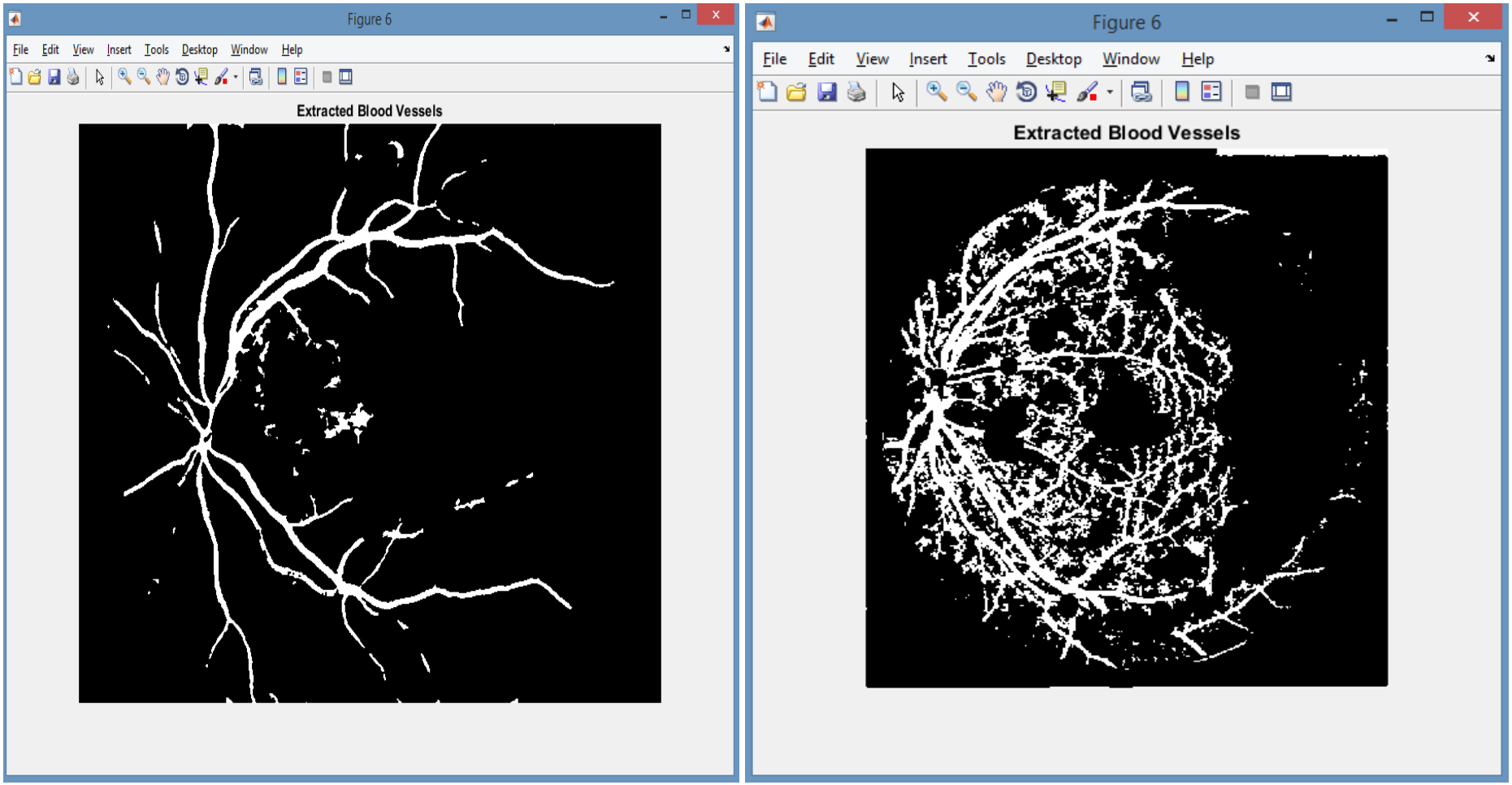

Figure 35: A Comparison of DR and Healthy Retinal Image Blood Vessels

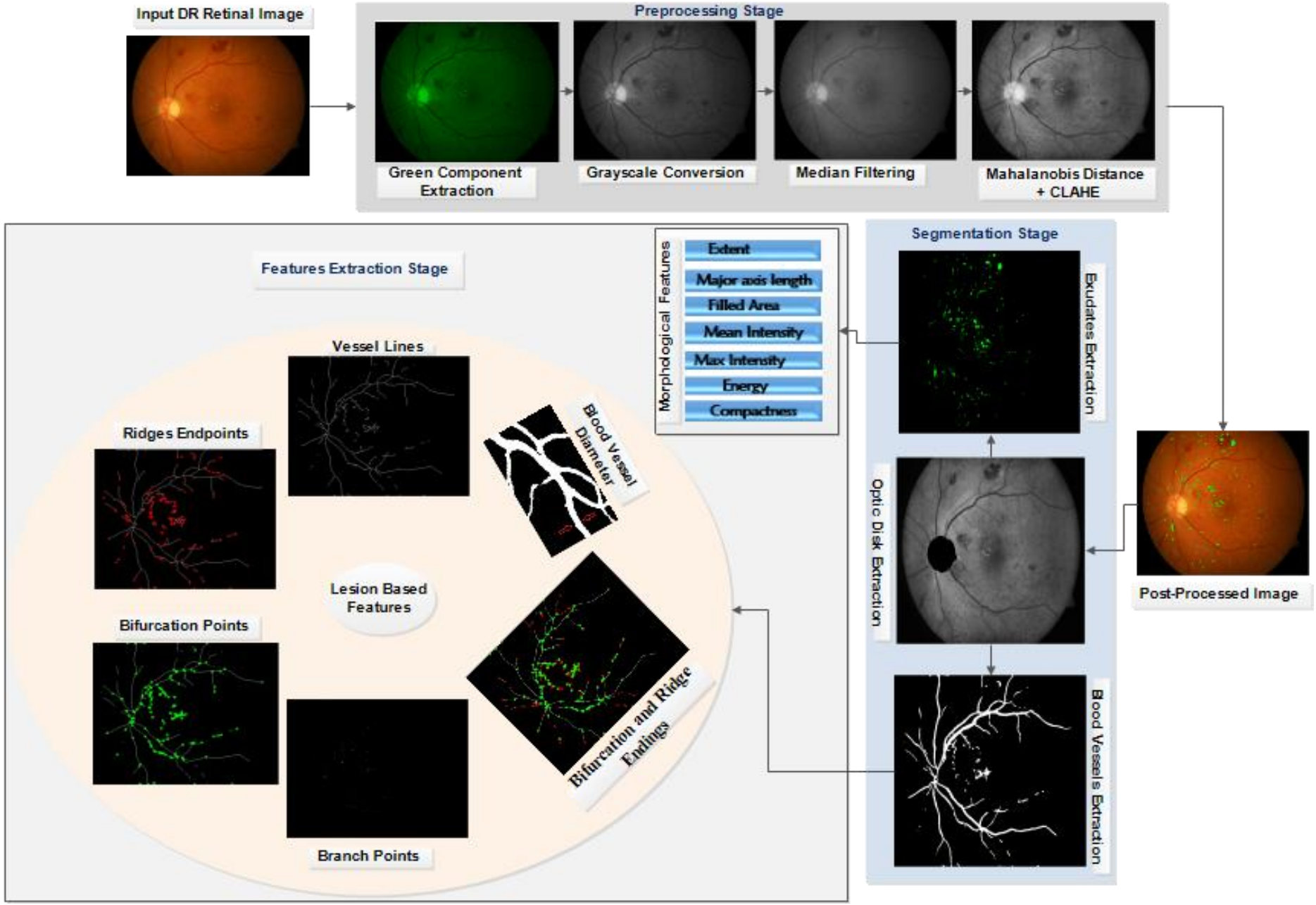

Figure 36: Overview of the DR Images Features Extraction Stage

12. REFERENCES

Abbadi, N. El, & Saadi, E. Al. (2014). BLOOD VESSEL DIAMETER. Journal of Computer Science, 10(5), 879–883. https://doi.org/10.3844/jcssp.2014.879.883

Abràmoff, M. D., Garvin, M. K., & Sonka, M. (2010). Retinal Imaging and Image Analysis. Biomedical Engineering, IEEE Reviews in, 3, 169–208. https://doi.org/10.1109/RBME.2010.2084567.Retinal

Adalarasan, R., & Malathi, R. (2018). Automatic Detection of Blood Vessels in Digital Retinal Images using Soft Computing Technique. Materials Today: Proceedings, 5(1), 1950–1959. https://doi.org/10.1016/j.matpr.2017.11.298

Akram, M. U., Tariq, A., Khan, S. A., & Javed, M. Y. (2014). Automated detection of exudates and macula for grading of diabetic macular edema. Computer Methods and Programs in Biomedicine, 114(2), 141–152. https://doi.org/10.1016/j.cmpb.2014.01.010

Alexandru, P. C., Johannes, K., & Alfred, M. (2012). ROBUST RETINA-BASED PERSON AUTHENTICATION USING THE SPARSE CLASSIFIER Alexandru Paul Condurache , Johannes Kotzerke and Alfred Mertins Institute for Signal Processing , University of L ¨ ubeck ubeck , Germany. In 20th European Signal Processing Conference (EUSIPCO 2012) Bucharest, Romania, August 27 - 31, 2012 (pp. 1514–1518).

Altomare, F., Kherani, A., & Lovshin, J. (2018). Retinopathy. Canadian Journal of Diabetes, 42, 210–216. https://doi.org/10.1016/j.jcjd.2017.10.027

Amin, J., Sharif, M., & Yasmin, M. (2016). A Review on Recent Developments for Detection of Diabetic Retinopathy. Scientifica, 2016. https://doi.org/10.1155/2016/6838976

Amin, J., Sharif, M., Yasmin, M., Ali, H., & Fernandes, S. L. (2017). A method for the detection and classification of diabetic retinopathy using structural predictors of bright lesions. Journal of Computational Science, 19, 153–164. https://doi.org/10.1016/j.jocs.2017.01.002

Arigbabu, O. A., Ahmad, S. M. S., Adnan, W. A. W., & Yussof, S. (2015). Integration of multiple soft biometrics for human identification. Pattern Recognition Letters, 68, 278–287. https://doi.org/10.1016/j.patrec.2015.07.014

Banerjee, S., & Kayal, D. (2016). Detection of hard exudates using mean shift and normalized cut method. Biocybernetics and Biomedical Engineering, 36(4), 679–685. https://doi.org/10.1016/j.bbe.2016.07.001

Barkana, B. D., Saricicek, I., & Yildirim, B. (2017). Performance analysis of descriptive statistical features in retinal vessel segmentation via fuzzy logic, ANN, SVM, and classifier fusion. Knowledge-Based Systems, 118, 165–176. https://doi.org/10.1016/j.knosys.2016.11.022

Barkhoda, W., Akhlaqian, F., Amiri, M., & Nouroozzadeh, M. (2011). Retina identification based on the pattern of blood vessels using fuzzy logic. EURASIP Journal on Advances in Signal Processing, 2011(1), 113. https://doi.org/10.1186/1687-6180-2011-113

Baumal, C. R. (2018). Imaging in Diabetic Retinopathy. Current Management of Diabetic Retinopathy. Elsevier Inc. https://doi.org/10.1016/B978-0-323-48452-7.00004-4

Bouacheria Mohamed, Benouadah Abdelmalek, Cherfa Yazid, Cherfa Assia & Belkhamsa Nourreddine (2018), "Non-Proliferative Diabetic Retinopathy Detection Using Mathematical Morphology", 2018 IEEE 4th Middle East Conference on Biomedical Engineering (MECBME), 219-224

Cofta, P., & Lacohée, H. (2008). Understanding public perceptions : trust and engagement in ICT-mediated services. International Engineering Consortium.

Daniel Koˇstialik, Luk´aˇs Maruniak & Martin Drahansk´ (2017), "Symptoms Detection in Eye Retina Image", 2017 IEEE symposium Series on Computational intelligence.

De Marsico, M., Frucci, M., & Riccio, D. (2016). An insight on eye biometrics. Pattern Recognition Letters, 82, 89–91. https://doi.org/10.1016/j.patrec.2016.05.003

Dehghani, A., Ghassabi, Z., Moghddam, H. A., & Moin, M. S. (2013). Human recognition based on retinal images and using new similarity function. EURASIP Journal on Image and Video Processing, 1(58), 1. https://doi.org/10.1186/1687-5281-2013-58

Dehghani, A., & Moghaddam, H. A. (2011). Retinal Identification Based on Rotation Invariant Moments. In 2011 5th International Conference on Bioinformatics and Biomedical Engineering (pp. 1–4). IEEE. Retrieved from http://ieeexplore.ieee.org/document/5780312/

Dunker, M. (2003). Dont Blink : Iris Recognition for Biometric Identification.

Ekka, B. K., Puhan, N. B., & Panda, R. (2015). Retinal Verification Using Point Set Matching, 159–163.

Fasanmade, O. A., & Dagogo-Jack, S. (2015). Diabetes Care in Nigeria. Annals of Global Health, 81(6), 821–829. https://doi.org/10.1016/j.aogh.2015.12.012

Figueiredo, I. N., Kumar, S., Oliveira, C. M., Ramos, J. D., & Engquist, B. (2015). Automated lesion detectors in retinal fundus images. Computers in Biology and Medicine, 66, 47–65. https://doi.org/10.1016/j.compbiomed.2015.08.008

Figueiredo, I. N., Moura, S., Neves, J. S., Pinto, L., Kumar, S., Oliveira, C. M., & Ramos, J. D. (2016). Automated retina identification based on multiscale elastic registration. Computers in Biology and Medicine, 79, 130–143. https://doi.org/10.1016/j.compbiomed.2016.09.019

Filiberto Altomare, Amin Kherani and Julie Lovshin (2018), “Retinopathy”, Canadian Journal of Diabetes, Vol. 42, Pp. 210–216

Franklin, S. W., & Rajan, S. E. (2014). Computerized screening of diabetic retinopathy employing blood vessel segmentation in retinal images. Biocybernetics and Biomedical Engineering, 34(2), 117–124. https://doi.org/10.1016/j.bbe.2014.01.004

Frucci, M., Riccio, D., Sanniti, G., & Serino, L. (2018). Using direction and score information for retina based person veriÞcation. Expert Systems With Applications, 94, 1–10. https://doi.org/10.1016/j.eswa.2017.10.044

Frucci, M., Riccio, D., Sanniti di Baja, G., & Serino, L. (2016). Severe: Segmenting vessels in retina images. Pattern Recognition Letters, 82, 162–169. https://doi.org/10.1016/j.patrec.2015.07.002

Geetharamani, R., & Balasubramanian, L. (2016). Retinal blood vessel segmentation employing image processing and data mining techniques for computerized retinal image analysis. Biocybernetics and Biomedical Engineering, 36(1), 102–118. https://doi.org/10.1016/j.bbe.2015.06.004

George, A., Karthick, G., & Harikumar, R. (2014). An Efficient System for Palm Print Recognition Using Ridges. In 2014 International Conference on Intelligent Computing

Applications (pp. 249–253). IEEE. https://doi.org/10.1109/ICICA.2014.60

Gupta, A., & Chhikara, R. (2018). ScienceDirect ScienceDirect Diabetic Retinopathy : Present and Past Diabetic Retinopathy : Present and Past. Procedia Computer Science, 132, 1432–1440. https://doi.org/10.1016/j.procs.2018.05.074

Hendrick, A. M., Gibson, M. V., & Kulshreshtha, A. (2015). Diabetic Retinopathy. Primary Care - Clinics in Office Practice. https://doi.org/10.1016/j.pop.2015.05.005

Holbura, C., Gordan, M., & Vlaicu, A. (2012). Retinal Vessels Segmentation using Supervised Classifiers Decisions Fusion. In Proceedings of 2012 IEEE International Conference on Automation, Quality and Tes 81 Robotics (pp. 185–190). IEEE. https://doi.org/10.1109/AQTR.2012.6237700

Hussain, A., Bhuiyan, A., Mian, A., & Ramamohanarao, K. (2013). Biometric security application for person authentication using retinal vessel feature. 2013 International Conference on Digital Image Computing: Techniques and Applications, DICTA 2013. https://doi.org/10.1109/DICTA.2013.6691489

Imani, E., & Pourreza, H. R. (2016). A novel method for retinal exudate segmentation using signal separation algorithm. Computer Methods and Programs in Biomedicine, 133, 195–205. https://doi.org/10.1016/j.cmpb.2016.05.016

Jagadiswary, D., & Saraswady, D. (2016). Biometric Authentication Using Fused Multimodal Biometric. Procedia Computer Science, 85(Cms), 109–116. https://doi.org/10.1016/j.procs.2016.05.187

Jain, A. K., Nandakumar, K., & Ross, A. (2015). 50 years of biometric research: Accomplishments, challenges, and opportunities. Pattern Recognition Letters. https://doi.org/10.1016/j.patrec.2015.12.013

Joshi, S., & Karule, P. T. (2018). A review on exudates detection methods for diabetic retinopathy. Biomedicine & Pharmacotherapy, 97(September 2017), 1454–1460. https://doi.org/10.1016/j.biopha.2017.11.009

Karunanayake, N., & Kodikara, N. D. (2015). An Improved Method for Automatic Retinal Blood Vessel Vascular Segmentation Using Gabor Filter. Open Journal of Medical Imaging, 5(5), 204–213. https://doi.org/10.4236/ojmi.2015.54026

Kauppi, T., Kalesnykiene, V., Kamarainen, J., Lensu, L., & Sorri, I. (2006). DIARETDB0 : Evaluation Database and Methodology for Diabetic Retinopathy Algorithms. Machine Vision and Pattern Recognition Research Group, Lappeenranta University of Technology, Finland. Retrieved from http://www.siue.edu/~sumbaug/RetinalProjectPapers/Diabetic Retinopathy Image Database Information.pdf

Kaur, J., & Mittal, D. (2018). A generalized method for the segmentation of exudates from pathological retinal fundus images. Integrative Medicine Research, 38(1), 27–53. https://doi.org/10.1016/j.bbe.2017.10.003

Keane, P. A., & Sadda, S. R. (2014). Retina 82 ging in the twenty-first century: State of the art and future directions. Ophthalmology, 121(12), 2489–2500. https://doi.org/10.1016/j.ophtha.2014.07.054

Köse, C., & Ikibaşs, C. (2011). A personal identification system using retinal vasculature in retinal fundus images. Expert Systems with Applications, 38(11), 13670–13681. https://doi.org/10.1016/j.eswa.2011.04.141

Kumar, M., & Rana, A. (2016). Image Enhancement using Contrast Limited Adaptive Histogram Equalization and Wiener filter. International Journal Of Engineering And Computer Science, 5(16977), 16977–16979. https://doi.org/10.18535/ijecs/v5i6.30

Kusakunniran, W., Wu, Q., Ritthipravat, P., & Zhang, J. (2018). Hard Exudates Segmentation based on Learned Initial Seeds and Iterative Graph Cut. Computer Methods and Programs in Biomedicine, 158, 1–32. https://doi.org/10.1016/j.cmpb.2018.02.011

Kwan, A. S., Barry, C., Franzco, I. L. M., & Franzco, L. C. (2006). Fluorescein angiography and adverse drug reactions revisited : the Lions Eye experience. Clinical and Experimental Ophthalmology, 34(1), 33–38. https://doi.org/10.1111/j.1442-9071.2006.1136.x

Lajevardi, S. M., Arakala, A., Davis, S. A., & Horadam, K. J. (2013). Retina verification system based on biometric graph matching. IEEE Transactions on Image Processing, 22(9), 3625–3635. https://doi.org/10.1109/TIP.2013.2266257

Lefohn, A., Budge, B., & Shirley, P. (2003). An Ocularist ' s Human Iris. IEEE Computer Graphics and Applications, 23(6), 70–75. https://doi.org/10.1109/MCG.2003.1242384

Li, X., & Wee, W. G. (2014). Retinal vessel detection and measurement for computer-aided

medical diagnosis. Journal of Digital Imaging, 27(1), 120–132. https://doi.org/10.1007/s10278-013-9639-y

Liu, Q., Zou, B., Chen, J., Ke, W., Yue, K., Chen, Z., & Zhao, G. (2017). A location-to-segmentation strategy for automatic exudate segmentation in colour retinal fundus images. Computerized Medical Imaging and Graphics, 55, 78–86. https://doi.org/10.1016/j.compmedimag.2016.09.001

Lumini, A., & Nanni, L. (2017). Overview of the combination of biometric matchers. Information Fusion, 33, 71–85. https://doi.org/10.1016/j.inffus.2016.05.003

Mahendran, G., & Dhanasekaran, R. (2015). Investigation of the severity level of diabetic retinopathy using supervised classifier algorithms. Computers and Electrical Engineering, 45, 312–323. https://doi.org/10.1016/j.compeleceng.2015.01.013

Mahesh, K. K., & Kashid, N. S. (2013). Review on Fundus Image Acquisition Techniques with Data base Reference to Retinal Abnormalities in Diabetic RetinopathyReview on Fundus Image Acquisition Techniques with Data base Reference to Retinal Abnormalities in Diabetic Retinopathy. International Journal of Computer Applications, 68(8), 975–8887.

Mapayi, T., Tapamo, J. R., Viriri, S., & Adio, A. O. (2016). Automatic retinal vessel detection and tortuosity measurement. Image Analysis and Stereology, 35(2), 117–135. https://doi.org/10.5566/ias.1421

Nakao, S., Yoshida, S., & Sonoda, K. (2018). Chapter 11 - An Overview of Diabetic Retinopathy. Nutritional and Therapeutic Interventions for Diabetes and Metabolic Syndrome (Second Edition). Elsevier Inc. https://doi.org/10.1016/B978-0-12-812019-4.00011-8

Nguyen, U. T. V, Bhuiyan, A., Park, L. A. F., & Ramamohanarao, K. (2013). An effective retinal blood vessel segmentation method using multi-scale line detection. Pattern Recognition, 46(3), 703–715. https://doi.org/10.1016/j.patcog.2012.08.009

Nigam, I., Vatsa, M., & Singh, R. (2015). Ocular biometrics: A survey of modalities and fusion approaches. Information Fusion, 26, 1–35. https://doi.org/10.1016/j.inffus.2015.03.005

Nixon, K., Aimale, V., & Rowe, R. (2008). Spoof detection schemes. Handbook of Biometrics, 403–423. https://doi.org/10.1007/978-0-387-71041-9_20

Panchal, P., Bhojani, R., & Panchal, T. (2016). An Algorithm for Retinal Feature Extraction Using Hybrid Approach. In Procedia Computer Science (Vol. 79, pp. 61–68). Elsevier Masson SAS. https://doi.org/10.1016/j.procs.2016.03.009

Panda, R., N.B., P., & Panda, G. (2017). Robust and accurate optic disk localization using vessel symmetry line measure in fundus images. Biocybernetics and Biomedical Engineering, 37(3), 466–476. https://doi.org/10.1016/j.bbe.2017.05.008

Panda, R., Puhan, N. B., & Panda, G. (2016). New Binary Hausdorff Symmetry measure based seeded region growing for retinal vessel segmentation. Biocybernetics and Biomedical Engineering, 36(1), 119–129. https://doi.org/10.1016/j.bbe.2015.10.005

Panwar, N., Huang, P., Lee, J., Keane, P. a., Chuan, T. S., Richhariya, A., … Agrawal, R. (2015). Fundus Photography in the 21st Century—A Review of Recent Technological Advances and Their Implications for Worldwide Healthcare. Telemedicine and E-Health, 22(AUGUST), 150826121255008. https://doi.org/10.1089/tmj.2015.0068

Pouya, N., & Pourghassem, H. (2017). A novel retina-based human identification algorithm based on geometrical shape features using a hierarchical matching structure. Computer Methods and Programs in Biomedicine, 141, 43–58. https://doi.org/10.1016/j.cmpb.2017.01.013

Prentašić, P., & Lončarić, S. (2016). Detection of exudates in fundus photographs using deep neural networks and anatomical landmark detection fusion. Computer Methods and Programs in Biomedicine, 137(Ispa), 281–292. https://doi.org/10.1016/j.cmpb.2016.09.018

Rahim, H. A., Ibrahim, A. S., Zaki, W. M. D. W., & Hussain, A. (2014a). Methods to enhance digital fundus image for diabetic retinopathy detection. Proceedings - 2014 IEEE 10th International Colloquium on Signal Processing and Its Applications, CSPA 2014, (Md), 221–224. https://doi.org/10.1109/CSPA.2014.6805752

Rahim, H. A., Ibrahim, A. S., Zaki, W. M. D. W., & Hussain, A. (2014b). Methods to Enhance Digital Fundus Image for Diabetic Retinopathy Detection. In Proceedings - 2014 IEEE 10th International Colloquium on Signal Processing and Its Applications, CSPA 2014 (pp. 221–224). https://doi.org/10.1109/CSPA.2014.6805752

Reza, M. N. (2018). Biomedical Signal Processing and Control Automatic detection of optic

disc in color fundus retinal images using circle operator. Biomedical Signal Processing and Control, 45, 274–283. https://doi.org/10.1016/j.bspc.2018.05.027

Rodrigues, L. C., & Marengoni, M. (2017a). Segmentation of optic disc and blood vessels in retinal images using wavelets, mathematical morphology and Hessian-based multi-scale filtering. Biomedical Signal Processing and Control, 36, 39–49. https://doi.org/10.1016/j.bspc.2017.03.014

Rodrigues, L. C., & Marengoni, M. (2017b). Segmentation of optic disc and blood vessels in retinal images using wavelets, mathematical morphology and Hessian-based multi-scale filtering. Biomedical Signal Processing and Control, 36, 39–49. https://doi.org/10.1016/j.bspc.2017.03.014

Rubaiyat, A. H. M., Aich, S., Toma, T. T., Mallik, A. R., & Rafat-Al-Islam. (2003). Fast normalized cross-correlation based retinal recognition. 2014 17th International Conference on Computer and Information Technology, ICCIT 2014, 358–361. https://doi.org/10.1109/ICCITechn.2014.7073086

Sabarigiri, B., & Suganyadevi, D. (2014). Counter Measures Against Iris Direct Attacks Using Fake Images and Liveness Detection Based on Electroencephalogram (EEG) Computer Sciences , Sree Saraswathi Thyagaraja College ,. World Applied Sciences Journal, 29, 93–98. https://doi.org/10.5829/idosi.wasj.2014.29.dmsct.17

Sadikoglu, F., & Uzelaltinbulat, S. (2016). Biometric Retina Identification Based on Neural Network. Procedia Computer Science, 102(August), 26–33. https://doi.org/10.1016/j.procs.2016.09.365

Sangita, B. (2017). Automatic segmentation of optic disk in retinal images. Biomedical Signal Processing and Control, 31, 483–498. https://doi.org/10.1016/j.bspc.2008.02.003

Sasidharan, G. (2014). Retina based Personal Identification System using Skeletonization and Similarity Transformation. International Journal of Computer Trends and Technology, 17(3), 144–147.

Senapati, R. K., Swain, G., V, R. B., & Prasad, P. M. . (2016). Computerized diabetic patients fundus image screening for lesion regions detection and grading. Biomedical Research:India 2016 Special Issue Special, 443–449.

Sidibé, D., Sadek, I., & Mériaudeau, F. (2015). Discrimination of retinal images containing bright lesions using sparse coded features and SVM. Computers in Biology and Medicine, 62, 175–184. https://doi.org/10.1016/j.compbiomed.2015.04.026

Sigursson, E. M., Valero, S., Benediktsson, J. A., Chanussot, J., Talbot, H., & Stefánsson, E. (2014). Automatic retinal vessel extraction based on directional mathematical morphology and fuzzy classification. Pattern Recognition Letters, 47, 164–171. https://doi.org/10.1016/j.patrec.2014.03.006

Slean, G. R., & Khurana, R. N. (2018). Classification of Diabetic Retinopathy. Current Management of Diabetic Retinopathy. Elsevier Inc. https://doi.org/10.1016/B978-0-323-48452-7.00003-2

Sudeshna Sil Kar and Santi P. Maity (2018), "Automatic Detection of Retinal Lesions for Screening of Diabetic Retinopathy", IEEE Transaction of Biomedical Engineering, Vol. 65, issue 3, Pp. 608-618.

Tian-Swee, T., Ameen, N. E., Hazabah, W. H., Yan-Chai, H., & Chong-Keat, T. (2015). Preprocessing Digital Retinal Images for Vessel Segmentation. Research Journal of Applied Sciences, Engineering and Technology, 14(1), 1–6. https://doi.org/10.19026/rjaset.14.3982

Unar, J. A., Seng, W. C., & Abbasi, A. (2014). A review of biometric technology along with trends and prospects. Pattern Recognition, 47(8), 2673–2688. https://doi.org/10.1016/j.patcog.2014.01.016

Usman Akram, M., Khalid, S., Tariq, A., Khan, S. A., & Azam, F. (2014). Detection and classification of retinal lesions for grading of diabetic retinopathy. Computers in Biology and Medicine, 45(1), 161–171. https://doi.org/10.1016/j.compbiomed.2013.11.014

Waheed, A., Akram, M. U., Khalid, S., Waheed, Z., Khan, M. A., & Shaukat, A. (2015). Hybrid Features and Mediods Classification based Robust Segmentation of Blood Vessels. Journal of Medical Systems, 39(10). https://doi.org/10.1007/s10916-015-0316-1

Waheed, Z., Usman Akram, M., Waheed, A., Khan, M. A., Shaukat, A., & Ishaq, M. (2016). Person Identification using Vascular and non-vascular Retinal Features. Computers and Electrical Engineering, 53, 359–371. https://doi.org/10.1016/j.compeleceng.2016.03.010

Wang, L., Liu, G., Fu, S., Xu, L., Zhao, K., & Zhang, C. (2016). Retinal image enhancement using robust inverse diffusion equation and self-similarity filtering. PLoS ONE, 11(7), 1–13. https://doi.org/10.1371/journal.pone.0158480

Wang, S., Yin, Y., Cao, G., Wei, B., Zheng, Y., & Yang, G. (2015). Hierarchical retinal blood vessel segmentation based on feature and ensemble learning. Neurocomputing, 149(PB), 708–717. https://doi.org/10.1016/j.neucom.2014.07.059

Watson, R. M., Machen, L., & Leiderman, Y. I. (2018). Clinical Diagnosis of Diabetic Retinopathy. Current Management of Diabetic Retinopathy. Elsevier Inc. https://doi.org/10.1016/B978-0-323-48452-7.00002-0

Welikala, R. A., Fraz, M. M., Dehmeshki, J., Hoppe, A., Tah, V., Mann, S., … Barman, S. A. (2015). Genetic algorithm based feature selection combined with dual classification for the automated detection of proliferative diabetic retinopathy. Computerized Medical Imaging and Graphics, 43, 64–77. https 87 .org/10.1016/j.compmedimag.2015.03.003

Xiong, L., & Li, H. (2016). An approach to locate optic disc in retinal images with pathological changes. Computerized Medical Imaging and Graphics, 47, 40–50. https://doi.org/10.1016/j.compmedimag.2015.10.003

Yin, B., Li, H., Sheng, B., Hou, X., Chen, Y., Wu, W., … Jia, W. (2015). Vessel extraction from non-fluorescein fundus images using orientation-aware detector. Medical Image Analysis, 26(1), 232–242. https://doi.org/10.1016/j.media.2015.09.002

Zhang, Y., Huang, D., Ji, M., & Xie, F. (2011). Image segmentation using PSO and PCM with Mahalanobis distance. Expert Systems with Applications, 38(7), 9036–9040. https://doi.org/10.1016/j.eswa.2011.01.041

Zhang, Z., Srivastava, R., Liu, H., Chen, X., Duan, L., Wing, D., & Wong, K. (2014). Open Access A survey on computer aided diagnosis for ocular diseases, 1–29.

Zhu, C., Zou, B., Zhao, R., Cui, J., Duan, X., Chen, Z., & Liang, Y. (2017). Retinal vessel segmentation in colour fundus images using Extreme Learning Machine. Computerized Medical Imaging and Graphics, 55, 68–77. https://doi.org/10.1016/j.compmedimag.2016.05.004